THE SHALLOW STRUCTURE OF THE MOON

by

Kenneth Robert Anderson

B.A., University of Pennsylvania
(1969)

SUBMITTED IN PARTIAL FULFILLMENT
OF THE REQUIREMENTS FOR THE
DEGREE OF MASTER OF
SCIENCE

at the

MASSACHUSETTS INSTITUTE OF TECHNOLOGY
May, 1972

Signature of Author _____
Department of Earth and Planetary Sciences

Certified by _____
Thesis Supervisor

Accepted by _____
Chairman, Departmental Committee on Graduate Students

ABSTRACT

The nature of the lunar seismic signal indicates the presence of two modes or propagation of seismic energy, one as relatively unscattered body waves through the interior of the moon and the other as intensely scattered energy through the near-surface layers. Travel-time and amplitude data from artificial impacts were used in conjunction with theoretical seismograms to determine the P-wave velocity structure to a depth of 100 km for the Oceanus Procellarum region. The important features of the model are: 1) rapid increase of velocity near the surface; 2) a discontinuity at a depth of about 25 km; 3) near-constant velocity (6.8 km/sec) between 25 and 65 km; 4) a major discontinuity at 65 km forming the base of the lunar crust; and 5) very high velocity (about 9 km/sec) below. Velocities in the upper layer of the crust match those of lunar basalts while those of the lower layer fall in the range of terrestrial gabbroic and anorthositic rocks.

ACKNOWLEDGEMENTS

Considering the nature of the "Moon Project" it is impossible to acknowledge everyone without whom this work would be impossible. I would like to thank Professors Nafi Toksoz and Frank Press for their careful discussion and prodding throughout this work, and Keiti Aki who was always willing to hear my crazy ideas. I also appreciate the help of the other members of the Passive Seismic Experiment Team, Gary Latham, James Dorman, David Lammlein and Fred Duennebier for sharing their thoughts and work on all three Apollo Missions with me. Four people made up the "critical mass" of the MIT lunar group: Ralph Wiggins, who provided me with the computer programs and know-how to help me analyze all aspects of the seismic data and who shared my delight in many things; Al Taylor, who contributed greatly with the massive data handling problems; Ed Stolper, whose perseverance, enthusiasm and insight were heartening when our results weren't; and Anton Dainty, whose discussion and insight in scattering and generalized ray theory problems is deeply appreciated. I would also like to thank Paul Reasenberg for being my anti-scientist (every scientist should have one), and my office-mates Ray Brown, Seymour Shlein, Michael Bouchon, Don Weidner,

Sean Solomon, Raul Maderiaga, and Jorge Mendiguren for their welcomed consolation and comic relief. I would like to thank Marti Finta for typing the original manuscript and for her many kindnesses and good cooking. Lastly, I would like to thank Herbie Smith for keeping the land-lady off my back in the final stages of this work.

This work was supported under NASA Grant (76218) and NASA Contract (73840).

TABLE OF CONTENTS

CHAPTER 1. INTRODUCTION

Despite the complicated nature of the lunar seismic signal, a velocity structure for the interior of the moon can be determined from the seismic data of the Apollo 12, 14, and 15 seismometers. Travel-times and amplitudes of compressional waves have been obtained from the impacts of the lunar module (LM) ascent stage and the fourth stage of the Saturn rocket booster (S-IV-B) for distances between 67 and 357 km. These data have been inverted to determine the seismic velocity structure for the first 100 km of the lunar interior using generalized ray theory.

Three seismic stations are presently working on the moon. Together they form an acute tripartite array in the central-equatorial regions of the moon (Fig. 1). Each station contains four seismometers. Three of them are aligned orthogonally to measure long-period horizontal (LPX and LPY) and vertical (LPZ) ground displacement. The fourth is a short-period vertical instrument (SPZ). The long-period seismometers are capacitance seismometers with a natural period of 15 sec (Latham et al., 1970). These are presently operated in a peaked-response mode with a natural frequency of about 2.4 sec. Figure 2 shows the step response of the instrument in the normal

and peaked modes. The short-period sensor has a resonant period of 1 sec. All seismometers can detect surface motion as small as 1 Å. The instruments can respond to a series of 15 commands sent from earth and control such functions as sensitivity, calibration, thermal state, frequency response, leveling and centering the seismometers.

The seismology of the moon is quite unlike that of the earth. Though the moon is seismically active, the seismic events are normally very low in amplitude, usually less than 1 on the Richter scale (Latham et al., 1971a, b). With only three stations, it is not possible to locate the epicenter and focal depths of these natural events with sufficient accuracy. Thirty stations on the near side of the moon would be necessary to match the density of stations on earth. Though the events often last for several hours, long-period surface waves or free oscillations from these small moonquakes have not been detected. Thus one must rely on six artificial impacts, of known location and origin time for the study of the lunar interior. In the next section the nature of the lunar seismic signals is briefly discussed. The data from the artificial impacts and its inversion is considered in the following section. The final section considers the signficance of the velocity model in the light of other work on the moon.

CHAPTER 2. NATURE OF THE LUNAR SEISMIC SIGNALS

The fact that the lunar seismograms are quite unlike normal earth seismograms has been well-documented (Latham et al., 1971 a,b). The major unusual features are: 1) the seismic signals show a gradual build-up in amplitude (on the order of 7 to 14 min) followed by a very gradual decay of amplitude that may last several hours (Fig. 3); 2) little correlation or coherence between components; 3) the envelope of the signal is highly modulated indicating energy arriving from multiple paths; 4) seismic phases in the first minute or so of the event are very weak and are usually closely followed by scattered arrivals.

Several authors, Nakamura (1970), Gold and Soter (1970), Pandit and Tozer (1970) and Berckhemer (1970), have shown that diffusion of seismic energy through a heterogeneous surface layer provides an adequate model for the gross features of the lunar seismogram. For an impact source, the major portion of the seismic energy is generated in the form of surface waves (Lamb, 1904). When the seismic velocity increases rapidly with depth, most of the energy will remain confined to the surface region with a small amount of energy slowly leaking into the interior.

That is, one can expect two modes of propagation, one

as intensely scattered waves through the heterogeneous surface region and the other as relatively unscattered (except at source or receiver) body waves through the interior of the moon. This effect can be seen most easily by comparing the envelopes of the artificial impacts. The LM impacts which are of comparable distance from the stations (67 to 114 km) all have similar envelopes showing a crude 1/r amplitude-distance relationship (Latham et al., 1971a). This indicates that most of the energy propagates through the near-surface scattering region. On the other hand, the S-IV-B of Apollo 13 (S-IV-B 13, Δ = 135 km) and the S-IV-B of Apollo 14 (S-IV-B 14, Δ = 172 km) impacts recorded at station 12 have quite different envelopes in their earlier portions. The amplitude of the S-IV-B 14 impact is a factor of two above the amplitude of the S-IV-B 13 impact for the first two minutes. However, the remainder of their envelopes are almost identical and agree with the 1/r scaling law. This indicates the earliest portion of the seismograms are dominated by body wave arrivals which travel faster than the later scattered arrivals. In the remainder of this section, we will consider the qualitative properties of the scattered portion of the seismograms and will consider the initial portion of the records in the following section. It turns out that the shortest portion of the lunar records provides us with the

most direct information about the interior.

Let us consider the model of a two-dimensional space of scatterers densely but uniformly distributed with seismic energy trapped in this space to determine, qualitatively, the seismic wave propagation in this type of medium. Nakamura (1970) has shown that the energy of the seismic signal at a distance r from the source and time t from the origin of the event will be:

$$E = (E_0/\pi\xi t) \exp (-r^2/\xi t - \omega t/Q) \qquad [1]$$

where E_0 is the initial seismic energy released at the soruce, ξ is the diffusivity of the medium in km /sec, ω is the frequency of the signal in radians/sec, and Q is the quality factor or the energy loss per cycle in the medium. Note that Eq. [1] is of the form of the random-walk distribution (Bartels, 1935). The seismic waves can be considered to propagate through the medium changing direction randomly upon being scattered. The terms of diffusion and mean-free path are used in the obvious analogy to the kinematic theory of gases in the limit of a very large number of scatterings. Since the diffusivity is equal to twice the average velocity of the seismic waves times the mean free-path, $\xi = 2vu$, the diffusivity will

increase (scattering decreases) with depth for a moon with increasing velocity with depth event if the mean free-path, u, (related to the number of scatters per unit area), remains constant. In addition, if one also assumes that the scatters are cracks, faults and brecciated zones due to meteorite impacting on the lunar surface (Latham et al., 1970) which heal (thus increasing u) with depth (Anderson and Warren, 1972) the effective scattering zone will be well-confined to the lunar surface.

In the initial stages of the study, a great deal of time was spent on determining the azimuth of natural events from the Apollo 12 sight (the only station available at the time) using the methods of Darbyshire (1963) and Stobach (1970), which have been successfully applied to locating microseismic sources on earth. The results were negative though many of the events analyzed were A_1 events (Latham et al, 1971b) which appear to come from the same source region. This analysis applied to man-made impacts of known location indicated the proper direction crudely and unreliably. The negative result of this experiment indicates that the diffusion model holds quite well for the lunar seismograms. It should be noted that there seemed to be some preferred orientation toward the north-east in a similar experiment done by Duennebier (1971) which

may indicate a structural trend in the scattering feature at the Apollo 12 site. Elston et al. (1971) have observed that linear surface features are aligned predominantly to the north, northeast, and northwest thus forming a "tectonic-grid" which could account for this orientation in the scattering.

The diffusion model also predicts the characteristics of the power spectra of the seismic signals. From the onset of the signals, the three components of particle motion are relatively uncorrelated. The coherence (Foster and Guinzy, 1967) of their power spectra is also quite low, generally 0.4 or less over all frequencies (0.0 to 2.5 Hz) for A_1 events. Seismic waves traveling through the scattering layer would be expected to undergo roughly the same number of scatterings and travel the same distance in a given length of time from the origin of the event. Therefore, the spectral content of the signal should depend only on time and not on epicentral distance or path to the station.

To test this idea, the power spectra for three time windows were computed using an overlapping summation technique (Gold and Raider, 1968) for the three S-IV-B impacts and the LM 14 impact recorded at station 12 (see Fig. 1 for their locations). The time windows chosen were the first minute from the first motion 6-11 and 10-15

min. into the event from the origin time (impact time). The vertical (Z) component power spectra for these events are shown in Fig. 4. The spectra are not corrected for the instrument response shown in Fig. 2. and the peak in the spectra at 0.45 Hz corresponds to the peak in the instrument response.

The impacts may be divided into two classes by their spectra. The LM 14, S-IV-B 13 and S-IV-B 14 impacts have a broad-band signal for the first minute followed by the absence of the higher frequencies later in time. The S-IV-B 15 impact has a broad spectrum for which high frequencies (0.7 to 1.2 Hz) predominate for at least the first 15 minutes of the event.

The fact that the early portion of the seismogram may differ in spectral content from the later portions supports the idea of two modes of propagation of seismic waves. The first portion being relatively unscattered body wave arrivals, the later portion being intensely scattered energy. The constancy of the spectral shape of the latter portion also supports this. The difference of the overall spectral shape between the first three impacts and the S-IV-B 15 indicates that source region and path does have an important effect on the spectral characteristics of the signal. Impacts in the Fra Mauro region and farther east will have more high-frequency energy than those impacts

closer to station 12.

There has been some discussion as to whether the scattering could be due to irregularities in the surface due to meteorite craters rather than a layer of scatterers several kilometers thick. Steg and Klemens (1970) have pointed out that Rayleigh waves scatter almost entirely into other Rayleigh waves of the same frequency but different direction when the scatterers are less than a wavelength or so below the surface. For surface irregularities, scattering varies as the fifth power of frequency, while for irregularities below the surface, scattering will increase more slowly with frequency and eventually decreasing with higher frequencies.

Latham et al. (1971a) have shown that the apparent diffusivity for the moon computed by fitting the envelope of the lunar seismograms to Eq. [1] is a function of both frequency and distance. Their Figure 6-18 shows that diffusivity is higher (scattering is less) for higher frequencies for a given distance and indicates that the effective thickness of the scattering layer is less for higher frequencies. For the two frequencies (1 Hz and 0.45 Hz) for which diffusivity was measured for several distances, there is a simple log-linear relationship. If these curves are extrapolated back to zero distance,

the diffusivity is higher for the lower frequency. This indicates, as one would expect, that most of the near-station (source) scattering is caused by surface irregularities.

It is interesting to compare lunar impact seismograms with their terrestrial analogs. Seismograms recorded close to nuclear events are one such analog since the nuclear event can be considered to be a near-surface point-source similar to lunar impacts and crustal seismic records are known to have codas of scattered energy which last two to three minutes from the first P arrival. The effect of Q can crudely be removed from the seismograms by multiplying the seismogram by a $e^{\pi f/Q}$ where f is the dominant frequency of the signal. This simple inverse Q filter was applied to several nuclear event records for distances comparable to those of lunar impact seismograms (240 to 285 km). An exampel of a raw seismogram and its inverse Q seismogram assuming a dominant frequency of 1.0 Hz and a Q of about 100 is shown in Fig. 4A. The envelope of the resulting signal remains relatively constant for the later portions of the signal which contains only scattered energy; thus a Q of 100 has removed most of the Q effect. The fact that once the Q effect has been removed, the scattered signal dominates the seismogram indicating that on earth as well as on the moon most of the seismic energy is scattered

energy. It is only the fact that the lunar Q is 10 to 30 times that of the earth's which allows the scattered signal to dominate the lunar records. Thus if the earth and the moon had comparable Q's one would expect their seismograms to be quite similar.

The nature of the lunar seismic signals shows that scattering is a very important phenomenon and that more research in this area is necessary before one can determine the effective depth of the scattering layer and the nature of the scatterers. The next section will show what can be inferred about the interior of the moon despite the complicated nature of the lunar seismograms.

CHAPTER 3. SEISMIC SIGNALS FROM ARTIFICIAL IMPACTS

The preceding section discussed the general characteristics of the lunar seismic signal and emphasized the existence of two modes of propagation of seismic energy in the moon. In this section, only the earliest portion of the seismograms will be considered. This portion of the seismograms is dominated by body waves which have traveled through the interior of the moon and will thus precede the intensely scattered energy which has propagated through the near-surface region of the moon at a slower velocity. Data from artificial impacts for which locations and origin times are known provide travel-time and amplitude data from which a velocity model for the interior can be inferred.

Signals from the impacts of S-IV-B and LM ascent stages have been recorded by three seismometers (Apollo 12, 14 and 15). The locations of the three operating stations and the artificial impacts' relevant distances and energies are listed in Table I. Locations of the stations and impacts are shown in Fig. 1. The S-IV-B impact precedes the lunar landing by about a day and thus is recorded by the stations operating prior to landing. The LM impact

which occurs after the lunar mission is completed can be recorded with the instrument of the same mission. The kinetic energy of a typical S-IV-B impact is about 13 times larger than a typical LM impact. First arrivals from LM impacts have been usable to a distance of 114 km, while those of S-IV-B impacts to a distance of 357 km.

The characteristics of all impact signals are very similar to each other. They all show the general characteristics of events discussed in the previous section. They are extremely prolonged with gradual build-up and very long exponential decay of signal intensity. These signals are always detectable for a few hours from the onset of the event.

The initial portions of the impact seismograms are shown in a montage plot in Fig. 5. The large amplitude and higher signal-to-noise ratio of S-IV-B impact records relative to those of the LM impacts are clearly illustrated. The change in the signal characteristics for records at different distances is also observed. Note the lack of sharp P and S wave arrivals typical of earth seismograms. The first arrivals are always much smaller in amplitude than the later portions of the seismograms.

The travel-times of first arrivals provide the most direct means of looking at the lunar interior. The arrivals

could be timed to an accuracy of about 0.2 sec where the signal-to-noise ratio is high. In other cases, uncertainties are 0.5 sec or greater. Multi-band filtered records were used to identify and time the arrivals. Particle motion plots were also used for identifying phases. The particle motion of the first arrivals is usually quite rectilinear with nearly vertical motion Secondary P arrivals (PP and PPP) are not quite so clearly indicated from particle motion. This is most likely due to the fact that the signal is already complicated by scattering from local features. Typical three-component seismograms filtered at two separate pass-bands are shown in Fig. 6. Note that the P wave stands out more clearly in vertical component high-pass traces, while the S waves and some later arrivals are clearer on lower frequency pass-band traces.

The travel-time-distance curve shown in Fig. 7a is a composite of P, PP and PPP arrivals measured from all impacts. Since both source and receiver are at the surface of the moon, the times can be plotted for phases such as PP and PPP on the same curve as the P arrivals by dividing the distance and travel-times by two for the PP and three for the PPP.

As a first step in determining a velocity model, these data were inverted, though of course any model derived

is highly non-unique. Models were derived which started with the known surface velocity of 0.1 km/sec (Kovach et al., 1971); Latham et al., 1971a) and joined the velocity smoothly to the depths for which travel-time data were available. In all models no low-velocity zones were allowed since only the simplest models could be justified by the sparse data available. These models show a rapid increase in velocity in the first 25 km to about 6 km/sec, followed by a more gradual increase to between 8 and 9 km/sec at a depth of 100 km. A plot of the velocity range of all the models computed is shown in Fig. 8. This can be used as a crude estimate of the "information content" of the data set, i.e., the range in which most reasonable velocity models are expected to fall.

One can observe from the montage plot of Fig. 5 that the amplitude of the first arrival of the S-IV-B 13 impact is quite different from that of the S-IV-B 14 impact though they are at similar distances from station 12 (135 and 172 km, respectively). The first arrival of the S-IV-B 13 impact is much lower in amplitude than the later P arrivals, whereas the onset of the S-IV-B 14 impact is much larger in amplitude (and longer in period) than the following portion of the seismogram. The incorporation of this amplitude information allows further refinement of the velocity model. Because the geometric focusing and

reflection of seismic rays are controlled by the velocity gradients of the interior, the amplitudes are sensitive indicators of velocity variations. A technique similar to that used by Helmberger and Wiggins (1971) was used to incorporate amplitude informations as well as travel-times into the velocity model.

A trial travel-time curve was sketched and a ray parameter, p, versus Δ curve was constructed from it ($P = dT/d\Delta$, the slope of the travel-time curve; Δ = distance in degrees). Constructing models in this plane has several advantages: The integral of the p versus Δ curve must give the correct travel-time for where there are observations and the slope of the curve can be used to control the amplitudes of the resulting model. The p versus Δ curve should be steep for large amplitude arrivals and nearly flat for small amplitdue arrivals. This representation is quite easy to use since models can be constructed and modified without the use of the computer excpet as a check. The p versus Δ curve is then inverted to a velocity model using the Wiechert-Herglotz integral (Grant and West, 1965; Gerver and Markushevich, 1966, 1967).

The amplitude data from both LM and S-IV-B impacts as well as the ray-theoretical amplitudes for the preferred

model are shown in Fig. 7b. The amplitudes have been scaled since the sources have different energies. An empirical correction (multiplication) factor of 20 for LM amplitudes was used. This value is larger than the square root of their energy ratios (Table I), however, since the S-IV-B's are much larger and impacts nearly vertical (67° from the horizontal as opposed to 3° for LM impacts), it is reasonable that the S-IV-B impacts are more efficient generators of seismic waves.

Note the agreement between the theoretical and observed amplitudes is quite good considering the experimental and theoretical limitations of the procedure. The ray diagram in Fig. 7c provides a more intuitive picture of the focusing multiplicity of the travel-time curve.

It should be pointed out that the use of the amplitude data is dependent on how each arrival is interpreted. As one can see from the travel-time curve, two triplications are included which may not be justified by the travel-time data alone. A more definitive approach to interpreting the lunar seismograms is to compute their theoretical equivalents. Generalized ray theory (Helmberger, 1968) has been used to compute synthetic seismograms for the impacts following a technique similar to that used by Helmberger

and Wiggins (1971). A brief discussion of generalized ray theory is provided in the appendix. This requires, in addition to the velocity structure of the moon, knowledge of the seismic source pulse due to the impact and the exact impulse response of the seismometer. In this representation, a seismic signal may be described by the convolution of three signals:

$$R(t) = S(t) * M(t) * I(t) \qquad [2]$$

where * denotes convolution, R(t) is the observed seismic signal, S(t) is the source shape, M(t) is the impulse response of the moon, and I(t) is the impulse response of the station. Helmberger and Wiggins have pointed out that S(t) is usually quite complicated and will include the secondary radiation due to irregularities close to the source. Similarly, I(t) can be expected to be more complicated than the simple impulse response of the instrument and will also incorporate properties of the material underlying the station. These complications should also be expected on the moon for a seismometer placed on its surface. Fortunately the structure of the interior and especially the velocity gradients and discontinuities play the most important role in controlling many of the charac-

teristics of the seismograms. By keeping S(t) and I(t) as constant as possible, one can isolate the structural contribution to the seismogram. For these purposes, three S-IV-B impact seismograms (Apollo 13, 14 and 15) recorded by the Apollo 12 station were chosen. This had the advantage of keeping the instrument response fixed and impact parameters nearly identical (Table I). LM impact seismograms were not considered because of their low signal-to-noise ratios.

The observed and computed seismograms at distances of 135, 172 and 357 km are shown in Fig. 9 and the corresponding velocity model in Fig. 10. One source function [S(t) * I(t)] was used for all of the computed seismograms. This source function is similar to the three initial broad cycles on the 172 km trace. This source has the same frequency as the instrument response and similar wave forms have been found on several natural moonquakes.

Note the general characteristics of the observed seismograms are very different. At 135 km, the first arrival is lower in amplitude than the later PP arrival and the peak that is the transition between them is broadened by the superposition of the end of the P arrival and the beginning of the PP arrival. At 172 km, the first arrival is a high amplitude pulse which is interpreted as a reflec-

ted arrival from a discontinuity at a depth of 65 km (the broadening of each cycle appears to be real and due to superposition of arrivals). This large arrival is immediately followed by the PP phase which is well-matched on the theoretical seismogram. The theoretical seismogram has a slight precursor due to a wave refracted from this discontinuity which is not apparent on the observed seismogram. This precursor is clearly visible on the 357 km seismogram, however, where it precedes the large reflected arrival by about 4 sec.

The overall agreement between the observed and theoretical records are very good although there are some discrepancies. The largest discrepancy is the lack of the high-frequency (1Hz) arrival, which begins roughly 8 sec after the first motion and which is most clearly shown in the 135 and 172 km events. Similar high-frequency arrivals can be seen on the other seismograms in Fig. 5 and have also been reported on the horizontal components at the Apollo 14 station by Latham et al. (1971a). They explained this as the arrival of shear waves converted from compressional waves at an interface below the instrument. Whatever its actual source, it is clear that scattering from near-receiver heterogeneities will contaminate the early portions of the seismograms. Key (1967, 1968) has reported scatter of first arrivals which can be associated

with known surface features near the receiver, a similar association may also be possible on the moon after further study.

The final velocity model shown in Fig. 10 takes into account all the data discussed above. Its main features are:

1. Very rapid increase in velocity at very shallow depths from a surface value of 0.1 km/sec (Kovach et al., 1971) to about 5km/sec at a 10 km depth.
2. A sharp increase at a depth of about 25 km.
3. Near constant value (about 7 km/sec) between 25 and 65 km.
4. A sharp increase at 65 km.
5. Very high velocity (greater than 9 km/sec) below the 65 km discontinuity (determined from a single data point at a distance of 357 km).

It is not possible to find suitable models without discontinuities given the interpretation of the arrivals described above. Some details of the model, such as the nature of the increase in velocity in the first 10 km cannot be determined without additional data closer than 67 km. The actual shapes of the discontinuities and the slope of the region of near-constant velocity can also be varied but travel times and especially the shapes of the

synthetic seismograms are drastically effected by any major change in this region of the velocity curve.

CHAPTER 4. COMPOSITIONAL IMPLICATIONS

The seismic data has provided us with evidence for the existence of a layered lunar crust (Fig. 10). In an analogy to the earth, one can define the base of the "lunar crust" to be the 65 km discontinuity. The velocity jump from 7 to 9 km/sec is very similar to that of the Mohorovicic discontinuity. The 65 km discontinuity occurs at a pressure of about 3.5 kb, which would be reached at a depth of about 10 km on earth, thus suggesting the analogy between this discontinuity and the base of the earth's oceanic crust.

High-pressure laboratory work on lunar and terrestrial rocks provide us with a way of inferring the composition of the lunar crust. A comparison of the seismic velocity model and the velocity versus depth curves for various lunar rocks is shown in Fig. 11. The velocity measurements have been made on lunar soils, breccias, and igneous rocks (Anderson et al., 1970; Kanamori, et al., 1970, 1971; Wang et al., 1971; and Warren et al., 1971). All of these rocks show very low velocities at low pressures compared to their terrestrial counterparts. This has been attributed to the absence of water in the

lunar rocks coupled with the effect of porosity and micro-cracks.

Using Fig. 11 as a guide, the following compositional units may be identified (Toksöz et al., 1972):

1. A near-surface layer of soil and broken rocks formed by the combined effect of meteorite impaction and pressure (Warren at al., 1971). The velocity increases very rapidly (from 0.1 km/sec) at the surface due to self-compaction under pressure.

2. Below a depth of about 2 km the velocities of lunar basalts fit the velocity profile to a depth of about 25 km. The velocity increases rapidly to a depth of about 10 km due to the closing of micro-cracks by pressure. The observed velocity model falls between the measured values of lunar rocks Nos. 10057 and 12065, paralleling these curves to a depth of 25 km. Unfortunately the present data does not provide any information about the nature of implacement of these basalts.

3. The 25 km discontinuity marks the beginning of the second crustal layer. This layer extends to a depth of about 65 km with nearly constant velocity throughout (6.8 to 7.0 km/sec). Figure 11 shows that no lunar rocks match the observed velocity. One must, therefore, resort to laboratory data on terrestrial rocks (see Press, 1966;

Anderson and Lieberman, 1966; for compilations). The examples plotted in Fig. 11 represent some possibilities. Note that gabbro, anorthosite and pyroxenite are possible candidates while velocities for eclogite are higher than those observed. Thus eclogite cannot be considered a likely possibility. Gabbro or anorthositic gabbro is most consistent with the petrogenesis of lunar basalts and other geophysical factors such as the mean density (3.34 gm/cc) and moment-of-inertia factor (0.402) for the moon (Toksöz et al., 1972).

4. The discontinuity at 65 km represents the next major structural boundary. The discontinuity is consistent with data from events at 172 km and 357 km, but the velocity jump to 9 km/sec is tentative since it is determined by only the 357 km seismogram. It is also important to point out that 9 km/sec is the "apparent" velocity. If the interface is dipping, true velocity might be higher or lower. Although not plotted, orthopyroxene and clinopyroxene-olivine rocks are acceptable candidates since they have the desired velocity and are favored from petrogenetic considerations (Ringwood and Essene, 1970; Green et al., 1971).

APPENDIX

Generalized ray theory is a method for calculating the exact surface response of a stratified half-space. The following will be a brief review on the rather involved theory. Only the most intuitive explanation will be provided. This explanation will be quite sufficient for understanding the use of generalized ray theory for determining velocity models from observed and synthetic seismograms which will be discussed later in the Appendix
The following is an annotated list of papers which provide a more detailed description of the theory:

Helmberger, 1967 and 1968 - A complete description of the theory and its use in determining the structure of the crust-mantle transition in the Bering Sea.

Spencer, 1960 - A presentation of generalized reflection and transmission coefficients for the case of two perfectly coupled half-spaces.

Dix, 1954 - An extremely careful presentation of Cagniard's method.

Helmberger and Wiggins, 1971 - Application of genera-

lized ray theory to determine the structure of the upper mantle of the midwestern United States. Their procedure is essentially the one followed in this paper.

As stated in Chapter 3, the synthetic seismogram R(t) for a distance r from the source can be considered as:

$$R(t) = S(t) * M(t) * I(t) \qquad [2]$$

where * denotes convolution, S(t) is the source function, M(t) is the impulse response of the model, and I(t) is the instrument response of the receiver. This Appendix wil will be concerned with the determination of M(t). Actually, the Cagniard-de Hoop method may be used to provide the step response for the mode, M'(t) and M(t) may be determined from

$$M(t) = \frac{dM'(t)}{dt} \qquad [A1]$$

In generalized ray theory, a seismogram is assumed to be the sum of the individual contributions from a set of "generalized rays." A generalized ray has two impor-

tant aspects which make it quite useful computationally. The amplitude of a particular ray is only dependent on the number of reflections and layer transitions the ray undergoes. That is, it is independent of the exact nature of the source (Spencer, 1960). Also, the effect of the reflected arrival and the refracted arrival from each layer is determined together. The step-response of the model is determined by a simple formalism which combines the effects of all of the rays.

Consider a typical layered model described by c_j, s_j, $\ _j$, Th_j, the P wave velocity, S wave velocity, density and thickness of each layer j respectively. A point-force used as a source generates a spectrum of both P and S waves. These waves, or generalized rays, are then followed through a number of reflections and mode conversions off the free surface and various layer interfaces. Each ray is described by the sequence of layers traversed, called segments, and the mode of propagation through each segment. Figure 12 shows several rays and their descriptions. Each segment description has the form mVn which means a segment "from the top of layer m to the top of layer n as a V wave", where m and n are layer numbers and V is either P or S. For example, lP2Pl is a P wave traveling through the first layer and represents both the

reflected and refracted wave. Since a ray may undergo P or S conversion at each interface, there will be 2^k rays of k segments.

The amplitude of a wave with ray-parameter p, $p = \sin \theta/c_j$, is given as the product of the generalized reflection and transmission coefficients corresponding to each segment of its path. (Spenser, 1960; Helmberger, 1968). For example, the ray 1P3S1 shown in Fig. 12 c would have the amplitude f(p), $f(p) = T_{p1p2}R_{p2s3}T_{s2s1}$, where T and R are the transmission and reflection coefficients for the corresponding interfaces and mode transitions. T and R are functions of p and are enumerated by Helmberger (1968). The travel-times of the ray is given by:

$$\tau(p) = pr + 2 \sum Th_j\eta_j \qquad [A2]$$

where $\eta_j = (\frac{1}{c_j^2} - p^2)^{1/2} = \cos \theta_j/c_j$. It is easy to see from the examples in Fig. 12 that different rays may have identical travel-times, such as 1P3S1 and 1S3P1. These rays are known as kinematically similar rays. Similarly, two rays will be dynamically similar if the product of reflection and transmission coefficients from

one ray is a permutations of the same product in the other. This allows some simplification in the summation since the response for equivalent rays need only be calculated once.

The model response is calculated as the sum of the effects of each ray. That is, $P(r,z,t)$, the vertical displacement due to a point step-function source of unit strength can be represented as:

$$P(r,z,t) = \sum_n P_n(r,z,t) \qquad [A3]$$

where $P_n(r,z,t)$ is the displacement due to each ray. Helmberger (1967) has shown that the Laplace transform of $P_n(r,z,t)$ can be written as:

$$\bar{P}_n(r,z,s) = \frac{i}{\pi} \int_\Gamma K_o(spr) f_n(p) \frac{p e^{-sg_n(p)}}{\eta_1} dp$$

where the overbar indicates the Laplace transform and s is the transform variable. K_o is the modified Bessel function, $f_n(p)$ is the product of the reflection and transmission coefficients for the ray and $g_n(p)$ equals $\sum_j Th_j \eta_j$. The contour is along the positive imaginary p-axis. The inversion of $\bar{P}(s)$ may be obtained by using the fact that $K_o(spr)e^{-sg_n(p)}$ is the Laplace transform of

$$\frac{H\left[\, t - pr - g_n(p) \,\right]}{\left[\left\{ t - g_n(p) \right\}^2 - p^2 r^2 \right]^{1/2}}$$

where H is the step function. Since the step function only has meaning when its arguments are real, the contour is deformed along such a path that

$$\tau = pr + g_n(p) \qquad [A5]$$

is real and positive. This contour, Γ', follows the positive Re(p)-axis and then leaves it along a hyperbolic path into the first quadrant as shown in Fig. 13. Each η_j will introduce a branch cut along the Re(p) from each $1/c_j$ to $+\infty$. We see that Eq. [A5] is the same as the travel-time for the ray as stated above, showing the relationship between p and t, the time along the seismogram. The seismogram is determined by summing over a range of p corresponding to the time interval of interest. The inverse transform of Eq. [A4] is then considered as a temporal convolution:

$$P_n(r,z,t) = \frac{2}{\pi} \operatorname{Im} \int^{t} \frac{p}{\eta_1} \frac{dp}{d\tau} \frac{f_n(p)H(t-\tau)}{(t-\tau)^{1/2}(t-\tau+2pr)^{1/2}} d\tau \qquad [A6]$$

where $dp/d\tau = \left[r - 2p \sum_j \frac{Th_j}{\eta_j} \right]^{-1}$. This integral is slowly varying along the contour Γ' except when $p(\tau)$ is near branch points or P_o, P_o being the point where the contour leaves the real axis.

It is interesting to consider the physical significnace of these points. The substitution of $p = 1/c_{n+1}$ and P_o into Eq. [A5] gives the P-refracted time and reflected time, respectively. Since the integrand of Eq. [A6] is real for $p < 1/c_{n+1}$ this portion of the integration contributes nothing. At $p = 1/c_{n+1}$, η_{n+1} becomes imaginary and the response begins. This corresponds to having no response before the first arrival.

The computation of the synthetic seismogram is calculated on the computer in the following steps:

1. Specification of a layered model.
2. Specification of the suite of rays of which the seismogram is to be composed.
3. Evaluation of Eq. [A6] for each ray until either the amplitude is negligible or it arrives out-

side the time of interest.

4. The step-response is differentiated, convolved with the source function and filtered in the frequency domain.

5. A plot of the resulting synthetic seismogram

When the proper number of rays are chosen, synthetic seismograms may be computed quite inexpensively. The remainder of this section will consider the use of such a program in the inversion of observed seismograms.

As pointed out in Chapter 3, the combination of travel-time and amplitude data with synthetic seismograms will produce the most meaningful velocity models. The inversion is done most easily using a combination of ray theory and generalized ray theory. Only ray-theoretical models which satisfy the travel-times and amplitudes will have their synthetic seismograms computed. The advantage of using ray theory is that it is usually simpler to understand the effect of changes in the models in terms of travel-times and amplitudes of the rays. Generalized rays add the unnecessary complication of the convolution of the response of each ray which needs only to be considered in the later stages.

The simplest procedure for determining a satisfactory ray theoretical model is to construct its p versus

Δ curve. Figure 14 shows the p-Δ curve for the model shown in Fig. 10. Though this may seem awkward at first, constructing models in this plane has several advantages. The integral of the p-Δ curve corresponds to the travel-time of the ray specified by the ray parameter p:

$$T(x) = p(x)x + \int_{p(x)}^{p(0)} x(p)dp \qquad [A7]$$

where T(x) is the travel-time of the ray p(x) arriving at the surface at point x (note the similarity between Eqs. [A7] and [A5]). Not only must Eq. [A7] provide the correct travel-time for each observation, but the slope of the p-Δ curve at these points can be used to control the amplitude of the arrival. It is well known that the ray-theoretical amplitude is determined by the absolute value of the second derivative of the travel-time curve, $|d^2T/d\Delta^2|$ (Bullen, 1965). However, variation of the curvature of the travel-time curve is rather difficult to interpret by eye and variations in a model may not show a noticeable variation in the curvature. It is much easier to use the slope of the p-Δ curve since $dp/d = d^2T/d\Delta^2$. The p-Δ curve should be steep for large amplitude arrivals and nearly flat for small amplitude

arrivals.

Figure 14 shows the p-Δ curve for the model of Fig. 10. The intersection of a vertical line from any distance with this curve will show the number of P arrivals to be expected and the area under the curve up to each point will be the travel-time from Eq. [A7] and the slope of the curve will indicate the amplitude. Since we are dealing with a surface source, the PP and PPP arrivals at a distance can be determined by drawing similar lines for half and a third of the distance, respectively. Such lines are indicated in Fig. 14 for several distances. A careful study of Fig. 14 will show that the resulting seismograms can be expected to be quite different from each other.

Using this procedure, curves which satisfy the travel-time and amplitude data can be constructed and modified without the use of the computer. The p-Δ curve can be inverted to a velocity model using the Wiechert-Herglotz integral (Grant and West, 1965; Bullen, 1965).

Synthetic seismograms for a layered model which is a close approximation to the continuous ray-theoretical model may now be constructed for various distances and source functions. It is best to compute seismograms for a range of distances since it is easier to interpret

the effects of various models over several seismograms. Helmberger and Wiggins (1971) provide a careful description of the effects of different models on synthetic seismograms. In general, a ray will contribute significantly to a seismogram for distances close to the critical distance which is the distance where the head wave first appears. Before the critical distance, only a reflected arrival will be observed. At the critical distance a large reflected arrival will be observed, followed by the separation of the refracted and reflected arrivals for larger distances. For distances beyond the critical distance the refracted arrival will lead the reflected arrival in time and its amplitude will diminish more rapidly with distance than the amplitude of the reflected arrival.

It is important to note that the above procedure still requires trial and error testing of models since the ray theoretical travel-times and amplitudes will be somewhat different than those on the synthetic seismograms. Arrival times are very similar, though the convolution with the source function will spread the arrival in time. The effects of discontinuities and steep gradients in the model may extend a few degrees farther than predicted by ray theory and the amplitudes of the synthetic seismo-

grams will be somewhat lower than predicted. The major reason for this is that ray theory assumes that the waves have infinite frequency whereas the synthetic seismogram is narrow-band filtered.

REFERENCES

Anderson, O.L. and Lieberman, R.C., Sound velocities in rocks and minerals: Vesiac state-of-the-art report, No. 7885-4-X, Willow Run Laboratories, University of Michigan, 182, 1966.

Anderson, O.L., Scholz, C., Soga, N., Warren, N., and Schreiber, E., Elastic properties of a microbreccia, igneous rock and lunar fines from Apollo 11 mission; Proceedings of the Apollo 11 Lunar Science Conference 3, Pergamon Press, New York, 1959.

Anderson, O.L. and N.W. Warren; Structure and Lunar seismology; The Moon, 1972 (in press).

Bartels, J.; Random fluctuations, persistences, and quasi-persistences in geophysical and cosmological periodicities; Terr. Magn. and Atmospher. Electr., 40, 1-60, 1935.

Berckhemer, H; A possible scattering mechanims for lunar seismic waves; Zeitschrift fur Geophysik, 36, 523-529, 1970.

Bullen, K.E.; An introduction to the theory of seismology; Cambridge University Press, Cambridge, England, p. 125, 1965.

Darbyshire, J.; A study of microseisms in South Africa; Geophys. J. R. Astr. Soc., 8, 165-175, 1963.

Dix, C.H.; The method of cagniard in seismic pulse problems; Geophysics, 29, 722-738, 1954.

Elston, W.E., A.W. Laughlin and J.A. Brower; Lunar nearside tectonic patterns from orbiter 4 photographs; J. Geophys. Res., 76, 23, 5670, 1971.

Foster, M.R. and N.J. Guinzy; The coefficient of coherence: its estimation and use in geophysical data processing; Geophysics, 32, 602-616, 1967.

Gerver, M.L. and V.M. Markushevich; Determination of a seismic wave velocity from the travel-time curve; Geophys. J. R. Astr. Soc., 11, 165-173, 1966.

Gerver, M.L. and V.M. Markushevich; On the characteristic properties of travel-time curves; Geophys. J. R. Astr. Soc., 13, 241-246, 1967.

Gold, Bernard and C.M. Rader; Digital processing of signals; McGraw Hill, New York, N.Y., 1969.

Gold, Thomas and Steven Soter; Apollo 12 seismic signal: indication of a deep layer of powder; Science, 169, 1071, 1970.

Green, D.H., Ringwood, A.E., Ware, N.G., Hibberson,W. O., Major, A., and Kiss, E.; Experimental petrology and petrogenesis of Apollo 12 basalts, Proceedings of the Second Lunar Science Conference 1, MIT Press, Cambridge, Mass., 610, 1971.

Grant, F.S. and G.F. West; Interpretation theory in applied geophysics, McGraw-Hill, New York, N.Y., p. 138, 1965.

Helmberger, D.V.; Head waves from the oceanic Mohorovichic discontinuity; Ph.D. thesis, University of California at San Diego, 1967.

Helmberger, D.V.; The crust-mantle transition in the Bering Sea; Bull. Seism. Soc. Amer., 58, 1, 179, 1968.

Helmberger, D. and R.A. Wiggins; Upper mantle structure of the midwestern United States; Jour. Geophys. Res., 76, 14, 3229, 1971.

Kanamori, H., Nur, A., Chung, D.H., Wones, D., and Simmons, G; Elastic wave velocities of lunar samples at high pressures and their geophysical implications; Science, 167, 726, 1970.

Kanamori, H., Mizutani, H., and Yamano Y.; Elastic wave velocity of Apollo 12 rocks at high pressures; The Proceedings of the Second Lunar Science Conference,3, The MIT Press, Cambridge, Mass., 2323, 1971.

Key, F.A.; Signal-generated noise recorded at the Eskdalemuir seismometer array station; Bull. Seis. Soc. Amer., 57, 1, 27-38, 1967.

Key, F.A.; Some observations and analysis of signal generated noise; Geophys. Jour., 15, 377-392, 1968.

Kovach, R.L., Watkins, J.S., and Landers, T.; Active seismic experiment; Apollo 14 Preliminary Science Report, NASA SP-272, 163, 1971.

Lamb, H.; On the propagation of tremors over the surface of an elastic solid; Phil. Trans. Roy. Soc. A203, 1-42, 1904.

Latham, G., Ewing, M., Dorman, J., Press, F., Toksoz, N., Sutton, G., Meissner, R., Duennebier, F., Nakamura, Y., Kovach, R. and Yates, M.; Seismic data from man-made impacts on the moon; Science, 170, 620, 1970.

Latham, G., Ewing M., Press, F., Sutton, G., Dorman, J., Nakamura, Y., Toksoz, N., Duennebier, F., Lammlein, D.; Passive seismic experiment; Apollo 14 Preliminary Science Report, NASA SP-272, 133, 1971a.

Latham, G., Ewing, M., Dorman, J., Lammlein, D., Press, F., Toksoz, N., Sutton, G., Duennebier, F. and Nakamura, Y.; Moonquakes; Science, 174, 687, 1971b.

Nakamura, Yosio; An interpretation of lunar seismic signals by intense scattering of surface waves; Abstract EOS, Fall 1970.

Pandit, B.I. and Tozer, D.C.; Anomalous propagation of elastic energy within the moon; Nature, 226, 5243, 335, 1970.

Press, F.; Seismic velocities; Handbook of Physical Constants, S.P. Clark Ed., Geol. Soc. Amer. Mem. 97, 195, 1966.

Ringwood, A.E., and E. Essene; Petrogenesis of Apollo 11 basalts, internal constitution and origin of the moon; Geochim. Cosmochim. Acta. Suppl. 1, 34, 769, 1970.

Spencer, T.W.; The method of generalized reflection and transmission coefficients; Geophysics, 25, 625-641, 1960.

Steg, R.G. and P.G. Klemens; Scattering of Rayleigh waves by surface irregularities; Phis. Rev. Let., 24, 8, 381, 1970.

Strobach, Klaus; Origin and properties of microseisms from the standpoint of oscillator theory; Bull. Seis. Soc. Amer., 55, 2, 365-390, April, 1965.

Toksoz, M.N., Press, F., Anderson, K. Dainty, A., Latham, G., Ewing, M, Dorman, J., Lammlein, D., Sutton, G., Duennebier, F. and Nakamura, Y.; Velocity structure and properties of the lunar crust; The Moon, 1972 (in press).

Wang, H., Todd, T., Weidner, D. and Simmons, G.; Elastic properties of Apollo 12 rocks; Proceedings of the Second Lunar Science Conference 3, MIT Press, Cambridge, Mass., 2327, 1971.

Warren, N., Schreiber, E., Scholz, C., Morrison, J.A., Norton, P.R., Kumazala, M. and Anderson, O.L.; Elastic and thermal properties of Apollo 12 and A Apollo 11 rocks; Proceedings of the Second Lunar Science Conference 3, MIT Press, Cambridge, Mass. 2345, 1971.

TABLE 1.

A. Coordinates of Seismic Stations and Impact Points and Relevant Distances.

Stations and Impacts	Coordinates (degrees)	Apollo 12 Site	Apollo 14 Site	Apollo 15 Site
Apollo 12 Site	3.04S 23.42W	-	-	-
Apollo 14 Site	3.65S 17.48W	181	-	-
Apollo 15 Site	26.08N 3.66E	1188	1095	-
Apollo 12 LM Impact	3.94S 21.20W	73	-	-
Apollo 13 S-IV B Impact	2.75S 27.86W	135	-	-
Apollo 14 S-IV B Impact	8.00S 26.06W	170	-	-
Apollo 14 LM Impact	3.42S 19.67W	114	67	-
Apollo 15 S-IV B Impact	1.36S 11.77W	357	186	-
Apollo 15 LM Impact	26.36N 0.25E	1130	1049	93

TABLE 1.

B. Impact Parameters

Impact	Date day-month-yr	Time (hr:min:sec)	Velocity (km/sec)	Mass (kg)	Kinetic Energy (ergs)	Angle from Horizontal (degrees)
Apollo 12 LM	20-11-69	22:17:17.7	1.68	2383	3.36×10^{16}	3.7
Apollo 14 LM	7-02-71	00:45:25.7	1.68	2303	3.25×10^{16}	3.6
Apollo 15 LM	3-08-71	03:03:37.0	1.70	2385	$3.44 \times ;0^{16}$	3.2
Apollo 13 S-IV B	15-04-70	01:09:41.0	2.58	13925	4.63×10^{17}	76
Apollo 14 S-IV B	4-02-71	07:40:55.4	2.54	14016	5.54×10^{17}	69
Apollo 15 S-IV B	29-07-71	20:58:42.9	2.58	13852	4.61×10^{17}	62

FIGURE CAPTIONS

Fig. 1 Apollo 12 and Apollo 14 seismic stations, impact points and seismic ray paths.

Fig. 2 Step response of the lunar seismographs. One digital unit is equal to 5 m V.

Fig. 3 Three LP components of S-IV-B 14 impact record on a compressed time scale. Note gradual rise and slow decay of the signal. This is characteristic of all impacts.

Fig. 4 Power spectra of the Z component for impacts recorded at ALSEP-12 for several time intervals. Each spectrum is plotted on the same relative amplitude scale (0.0 to 1.0) but have been shifted upwards for display purposes. The spectra are uncorrected for the instrument response. The dominant peak at .45 Hz corresponds to the instrument response peak (Fig. 2). The time window over which each spectrum is taken

is indicated to the right of each curve. 1 signifies the first minute from first motion. 6-11 is minutes 6 - 11 from the impact time, etc. Note the high frequency content of the first minute and the constancy of the spectra later in time.

Fig. 4A Removal of the effect of Q from an earth seismogram. Top trace is a narrow band (1.0 Hz) trace (and its envelope) of the nuclear test Half Beak recorded at a distance of 310 km. Approximate arrival times of the P, S, and Rayleigh waves are indicated. The bottom trace is after inverse Q filter has been applied as described in the text using Q = 107, f = 1.0 Hz.

Fig. 5 A montage plot of vertical components of seismograms recorded from all artificial impacts. Notation "LM 14 at 14" means LM-14 impact recorded at Apollo 14 station. "dmax" is the amplitude normalization; to obtain true relative amplitudes, seismogram amplitudes must be multiplied by this factor. Distance is in degrees; 1 degree = 30.3·km. Arrows indicate the first

arrival. Note the change of character of the seismograms with distance.

Fig. 6 Seismograms of Apollo 13, 14 and 15 S-IV-B impacts recorded at the Apollo 12 station. R, T, and Z indicate radial, transverse and vertical components of the motion, respectively. Each seismogram is band-pass filtered at two period intervals: 1-4 seconds and 3-15 seconds. P, PP, PPP, S and SS arrivals are shown.

Fig. 7 Travel time, amplitudes and ray paths. "Second arrival P" denotes a relatively large amplitude pulse that arrives after P which is associated with a travel time cusp. PP and PPP are surface reflected phases. Lines are theoretical curves for the velocity model given in Fig. 10. Note the large amplitudes associated with travel time cusps. "D.U." signifies digital unit. Seismic ray paths inside the moon correspond to the model shown in Fig. 10. Ray crossings correspond to multiplication of travel times. High density of rays indicates focusing

of energy and hence large amplitudes.

Fig. 8 Region of acceptable travel time models assuming a rapid increase in velocity from the surface and no low-velocity zones. Incorporating amplitude data restricts the range of acceptable models.

Fig. 9 Observed (solid line) and synthetic (dashed line) seismograms for three S-IV B impacts recorded at station 12. The change in seismic pulse shapes and relative amplitudes of first and later arrivals with increasing distance is obvious. At 357 km the first two peaks of the observed seismogram are noise pulses and can be clearly identified as such in unfiltered seismograms.

Fig. 10 Compressional velocity versus depth profile for the Fra Mauro region of the moon (see Fig. 1).

Fig. 11 Observed velocity profile and velocities of lunar and terrestrial rocks measured in the laboratory as a function of pressure. On the left, lunar rocks are identified by sample number.

"Terrestrial basalts" is an average value for basalts of the earth. On the right, all laboratory data are terrestrial. Two curves for each rock type mark the typical lower and upper boundaries of velocities for such rock types.

Fig. 12 Examples of ray-path descriptions.

Fig. 13 Complex p-plane showing path of integration and branch cut positions.

Fig. 14 p vs. Δ curve for the velocity model shown in Fig. 10.

Fig. 1

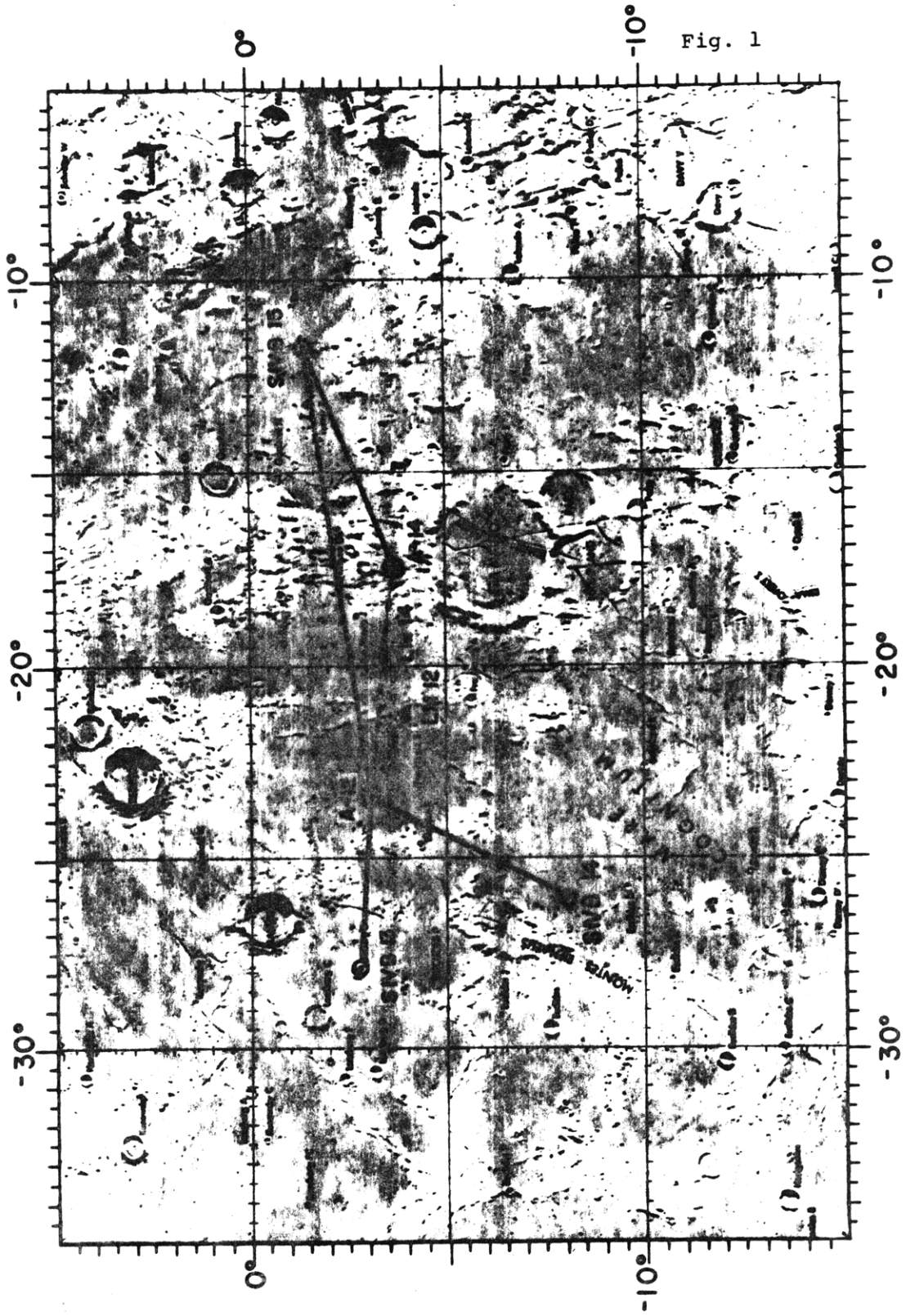

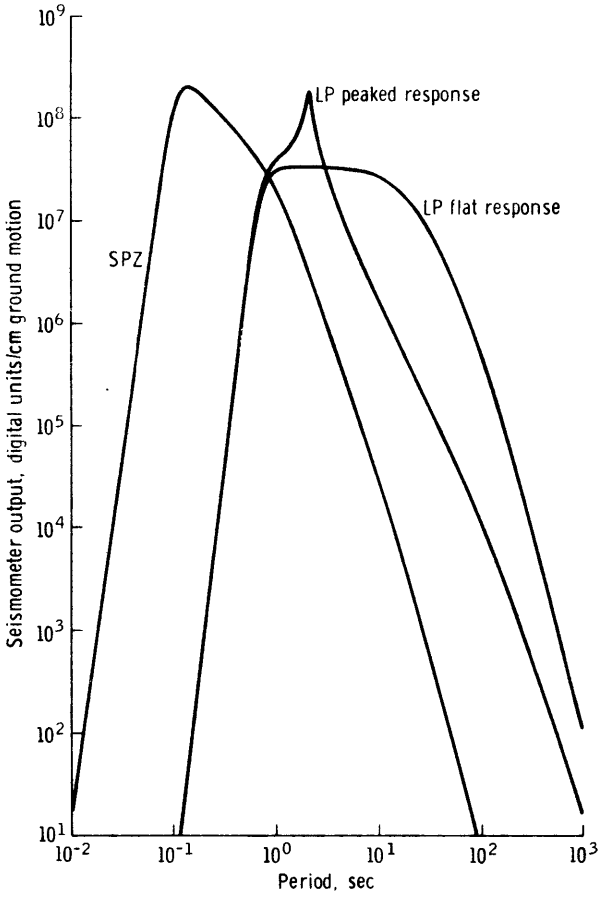
LP peaked response
LP flat response
SPZ
Seismometer output, digital units/cm ground motion
Period, sec
10^9
10^8
10^7
10^6
10^5
10^4
10^3
10^2
10^1
10^{-2}
10^{-1}
10^0
10^1
10^2
10^3

Fig. 2

Fig. 3

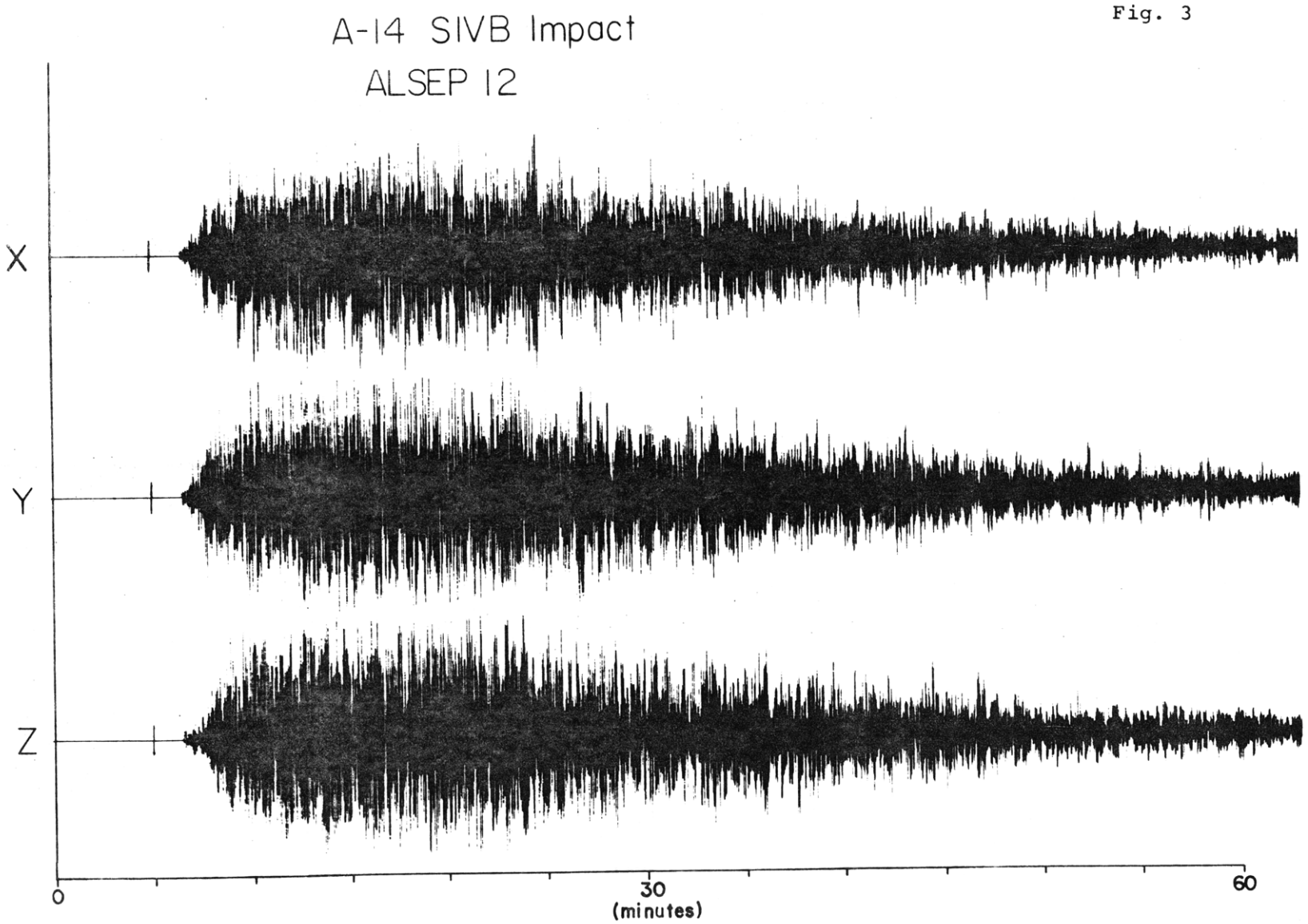

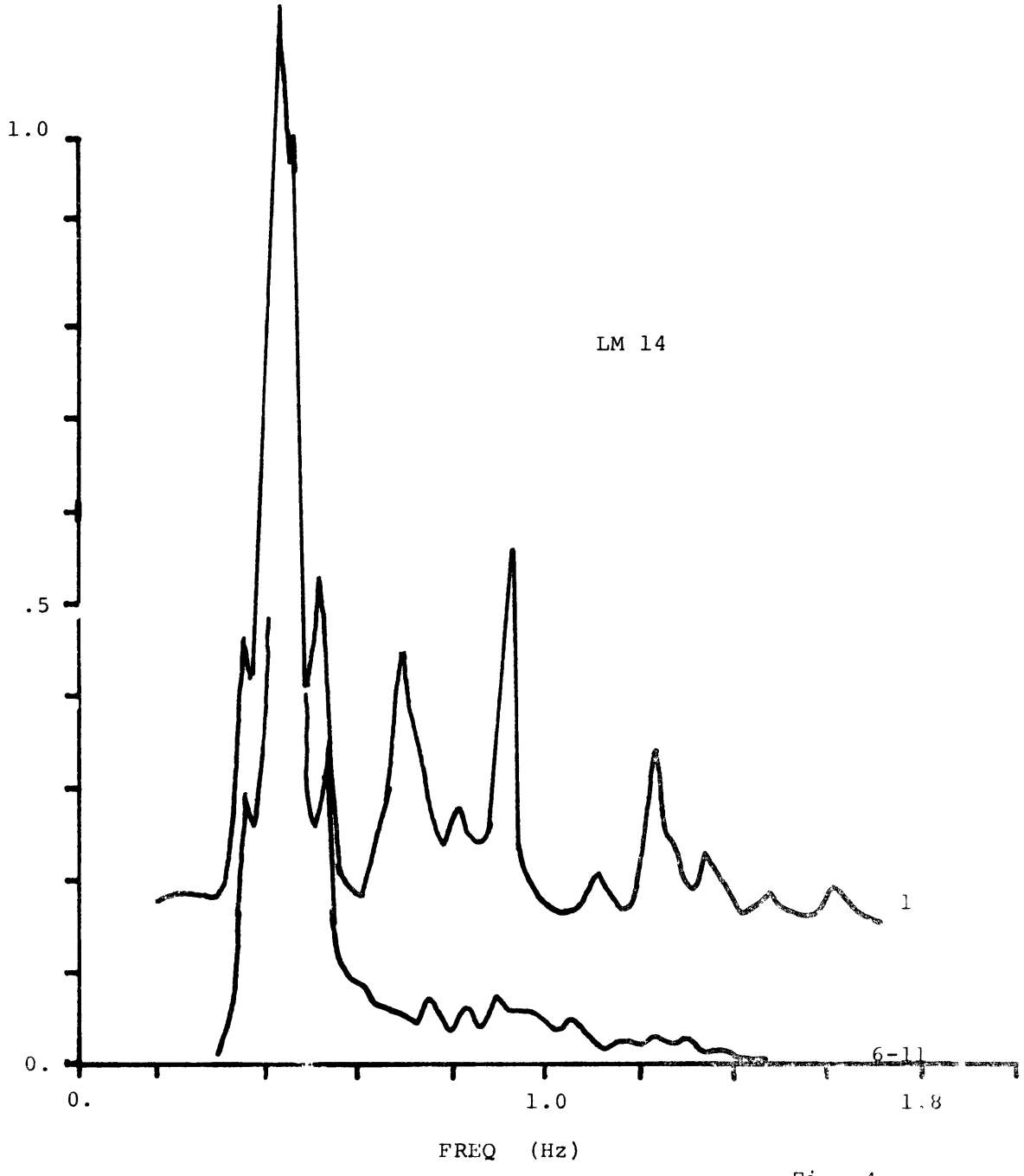

Fig. 4a

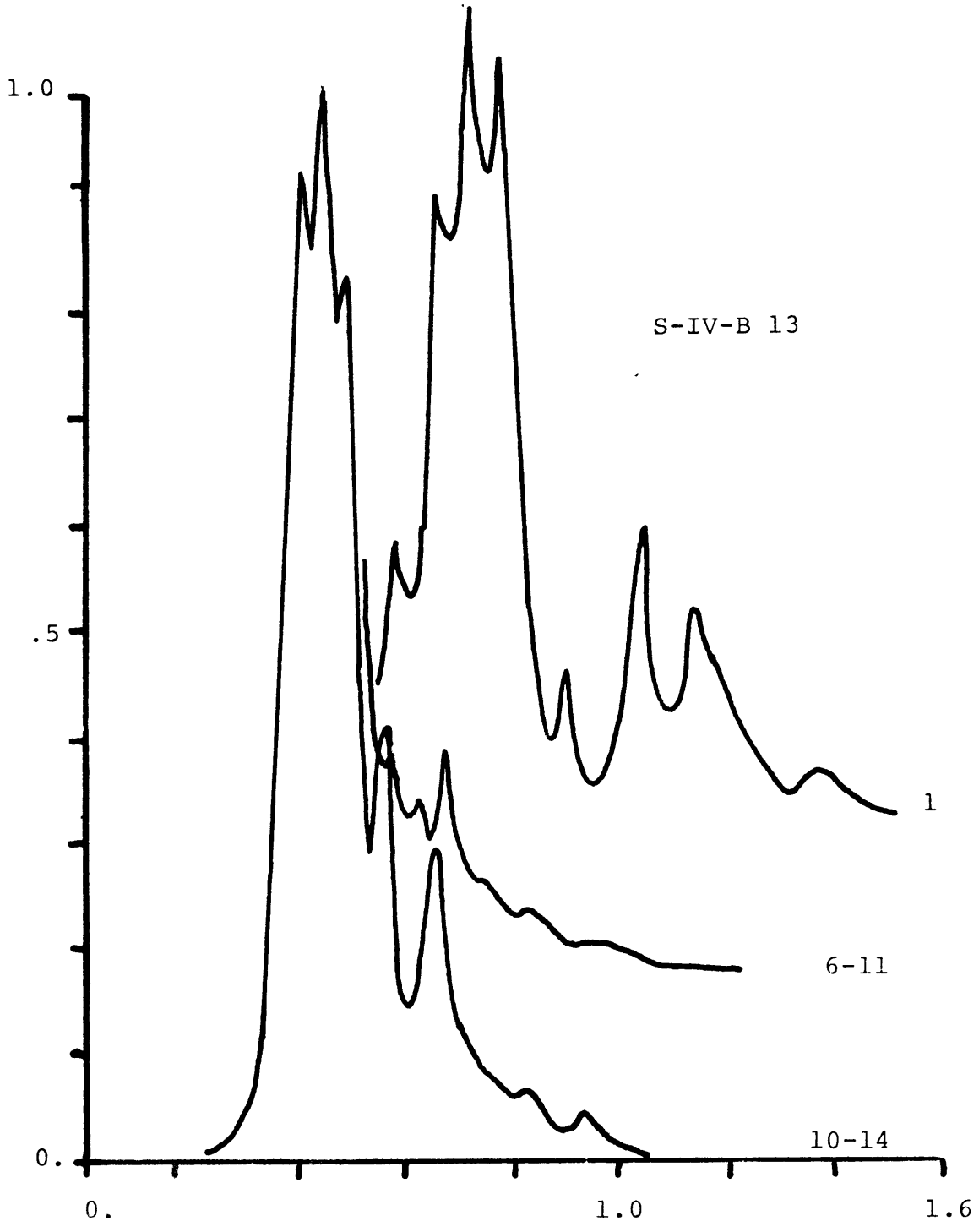

Fig. 4b

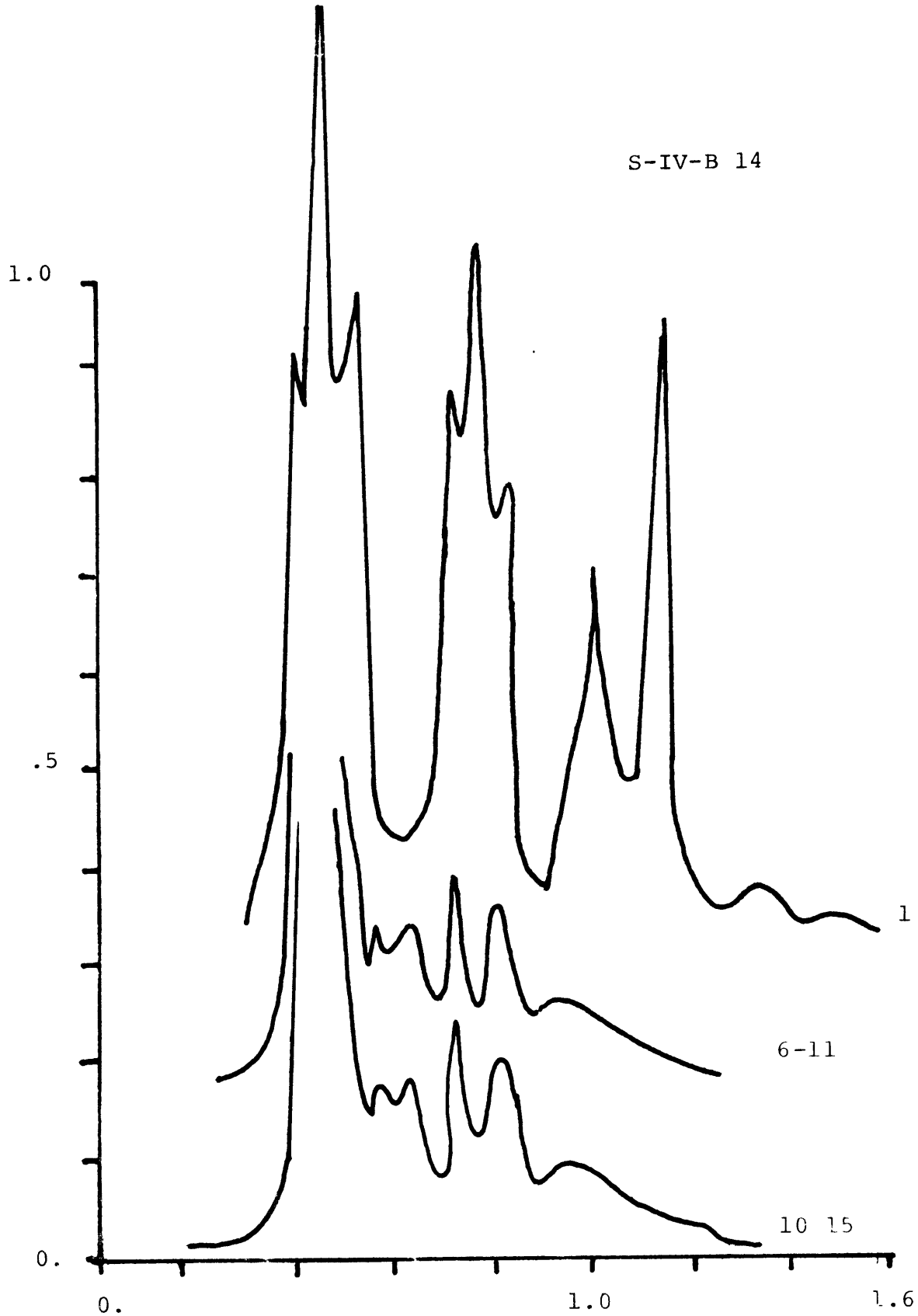

Fig. 4c

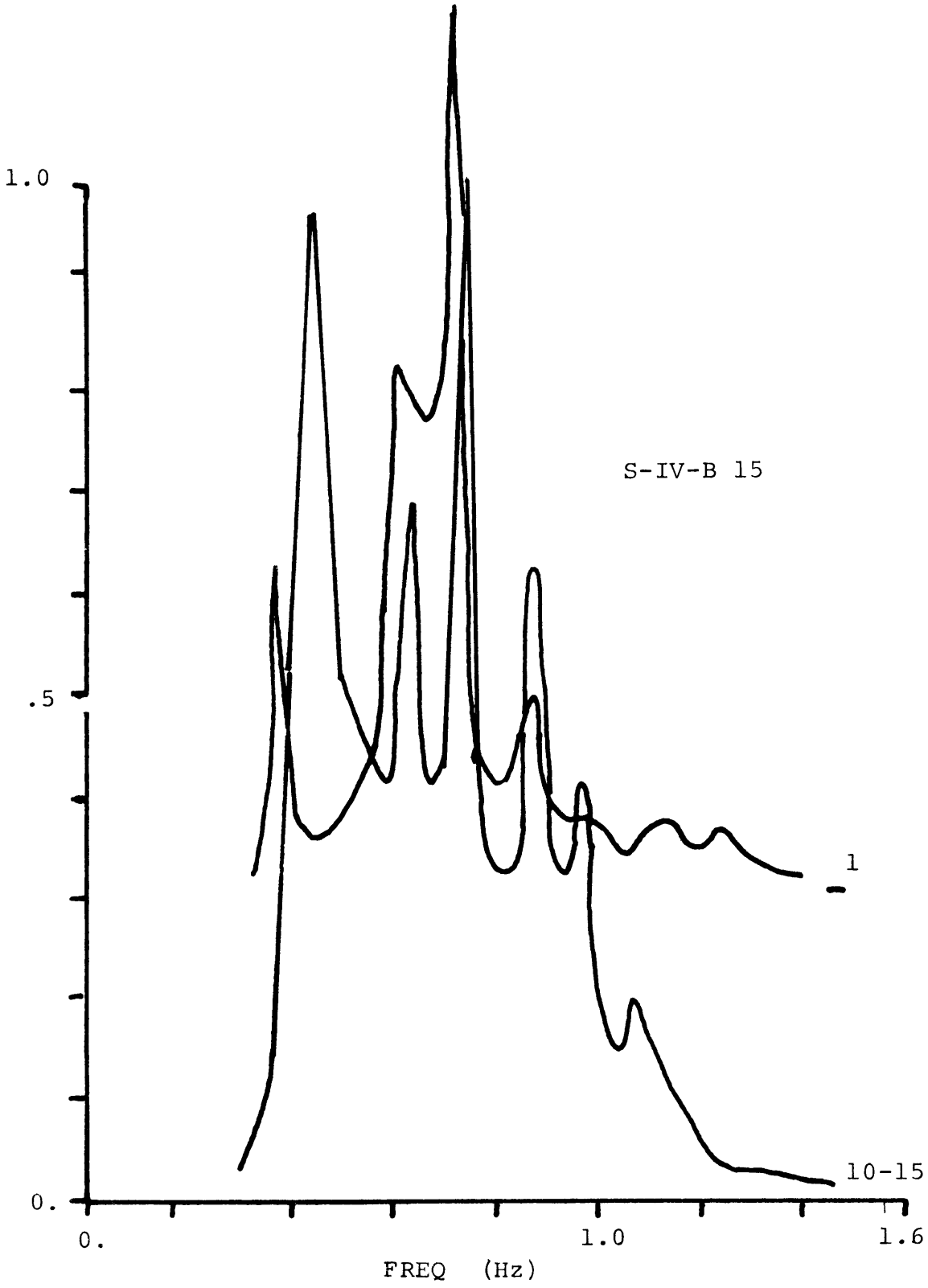

Fig. 4d

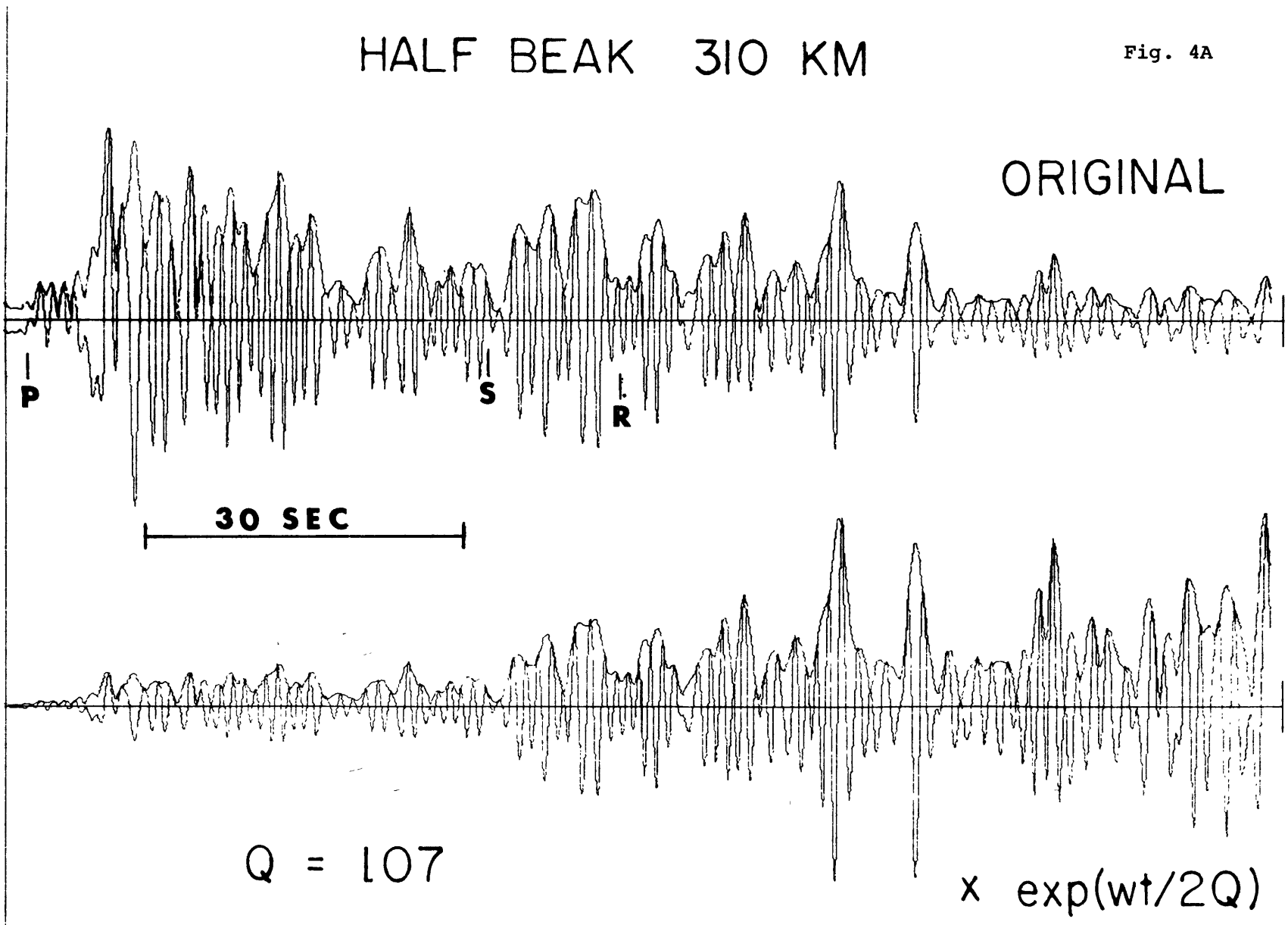

Fig. 4A

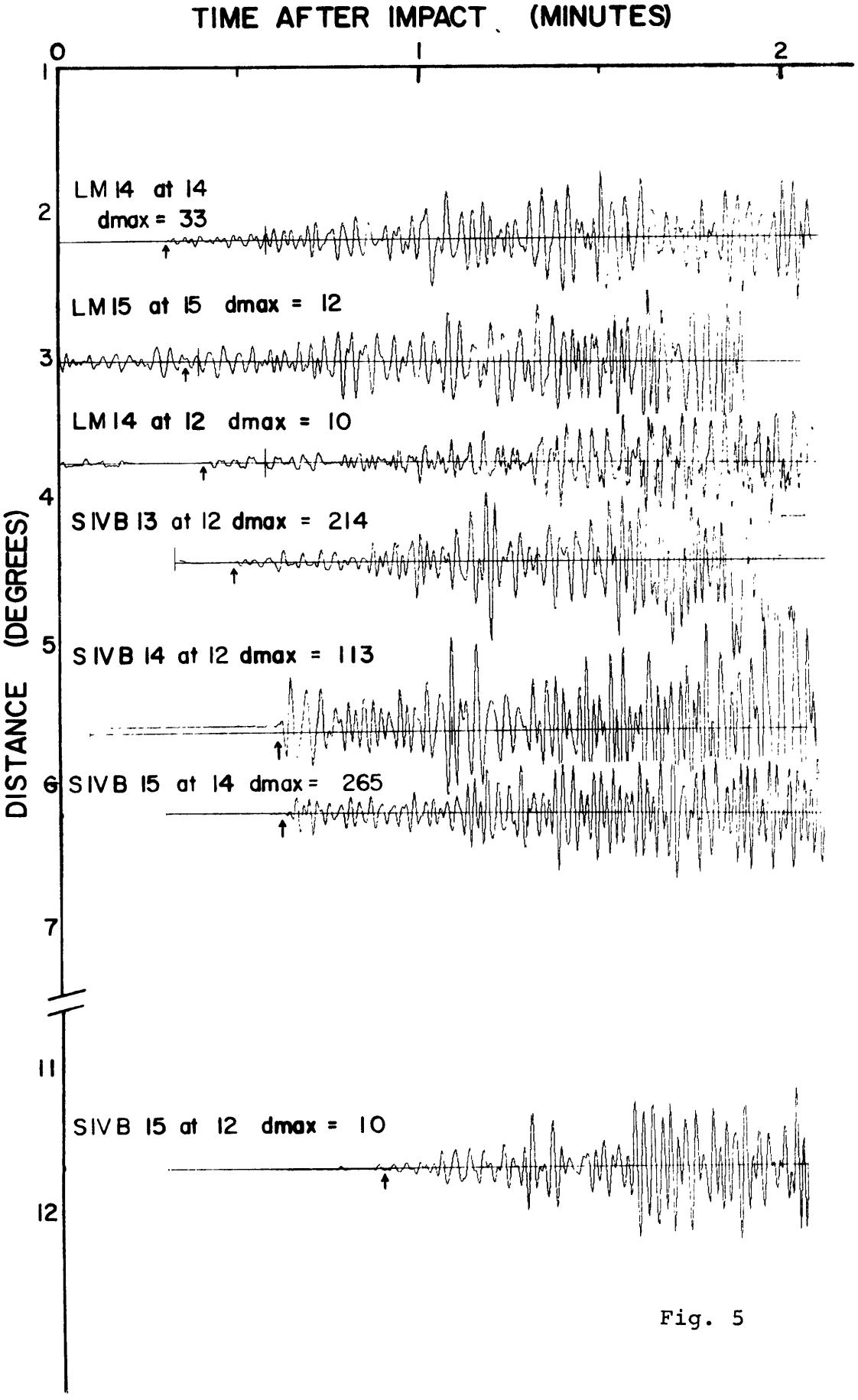
TIME AFTER IMPACT (MINUTES)
0
1
2
DISTANCE (DEGREES)
1
2
3
4
5
6
7
11
12
LM 14 at 14
dmax = 33
LM 15 at 15 dmax = 12
LM 14 at 12 dmax = 10
SIVB 13 at 12 dmax = 214
SIVB 14 at 12 dmax = 113
SIVB 15 at 14 dmax = 265
SIVB 15 at 12 dmax = 10

Fig. 5

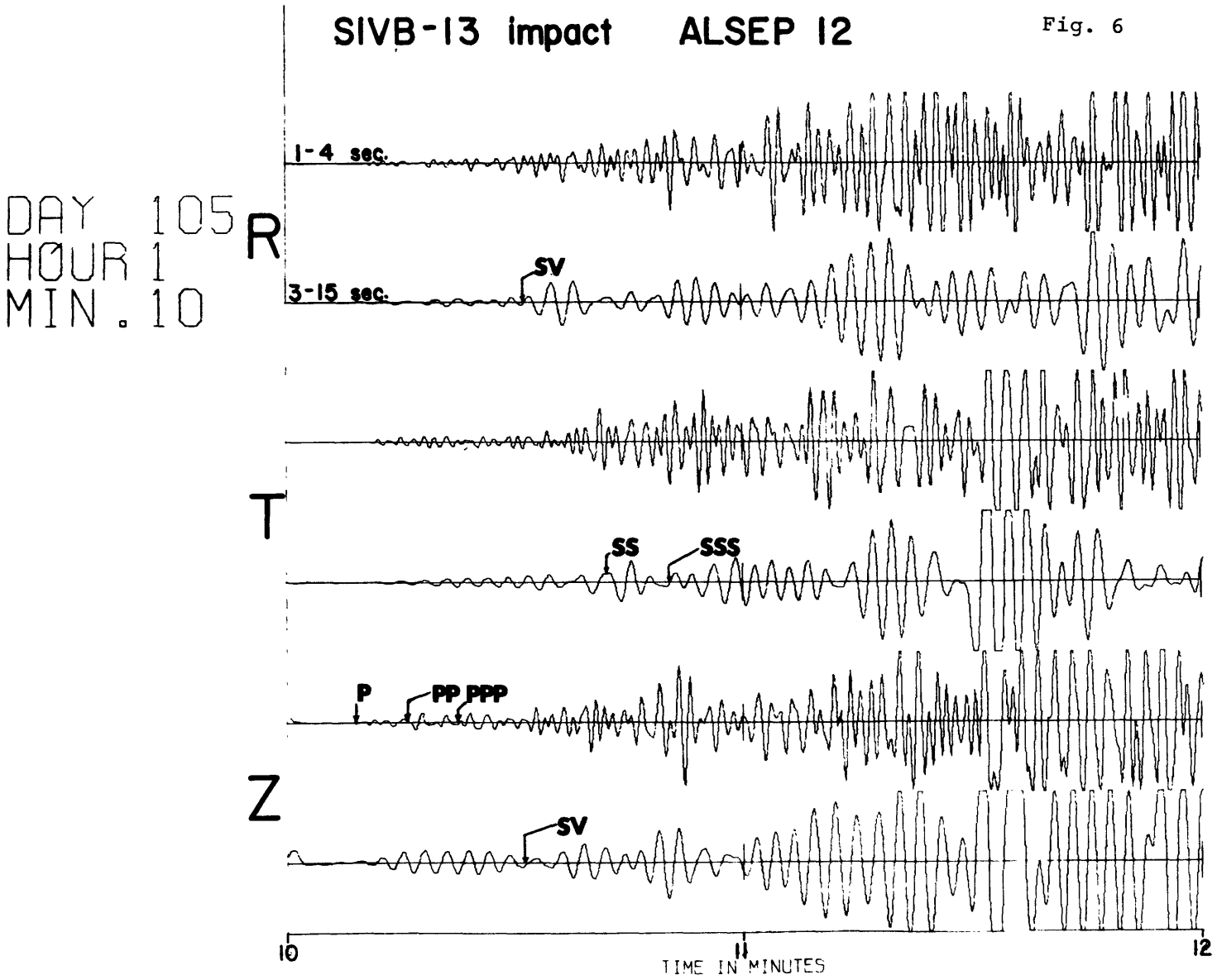
SIVB-13 impact ALSEP 12
DAY 105
HOUR 1
MIN. 10
R
T
Z
1-4 sec.
3-15 sec.
SV
SS
SSS
P
PP
PPP
SV
10
11
12
TIME IN MINUTES

Fig. 6

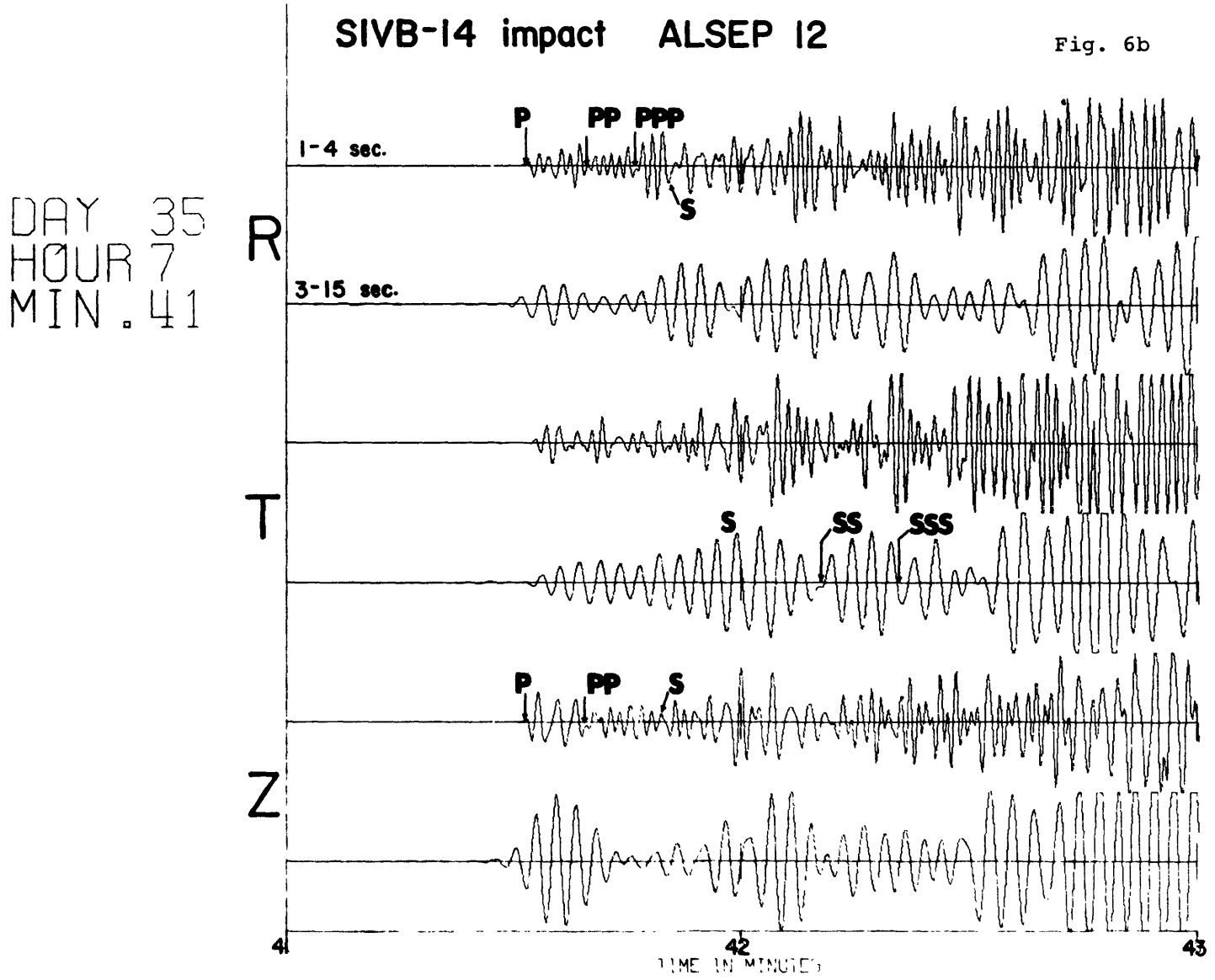
SIVB-14 impact ALSEP 12
DAY 35
HOUR 7
MIN. 41
R
T
Z
1-4 sec.
3-15 sec.
P
PP
PPP
S
SS
SSS
41
42
43
TIME IN MINUTES

Fig. 6b

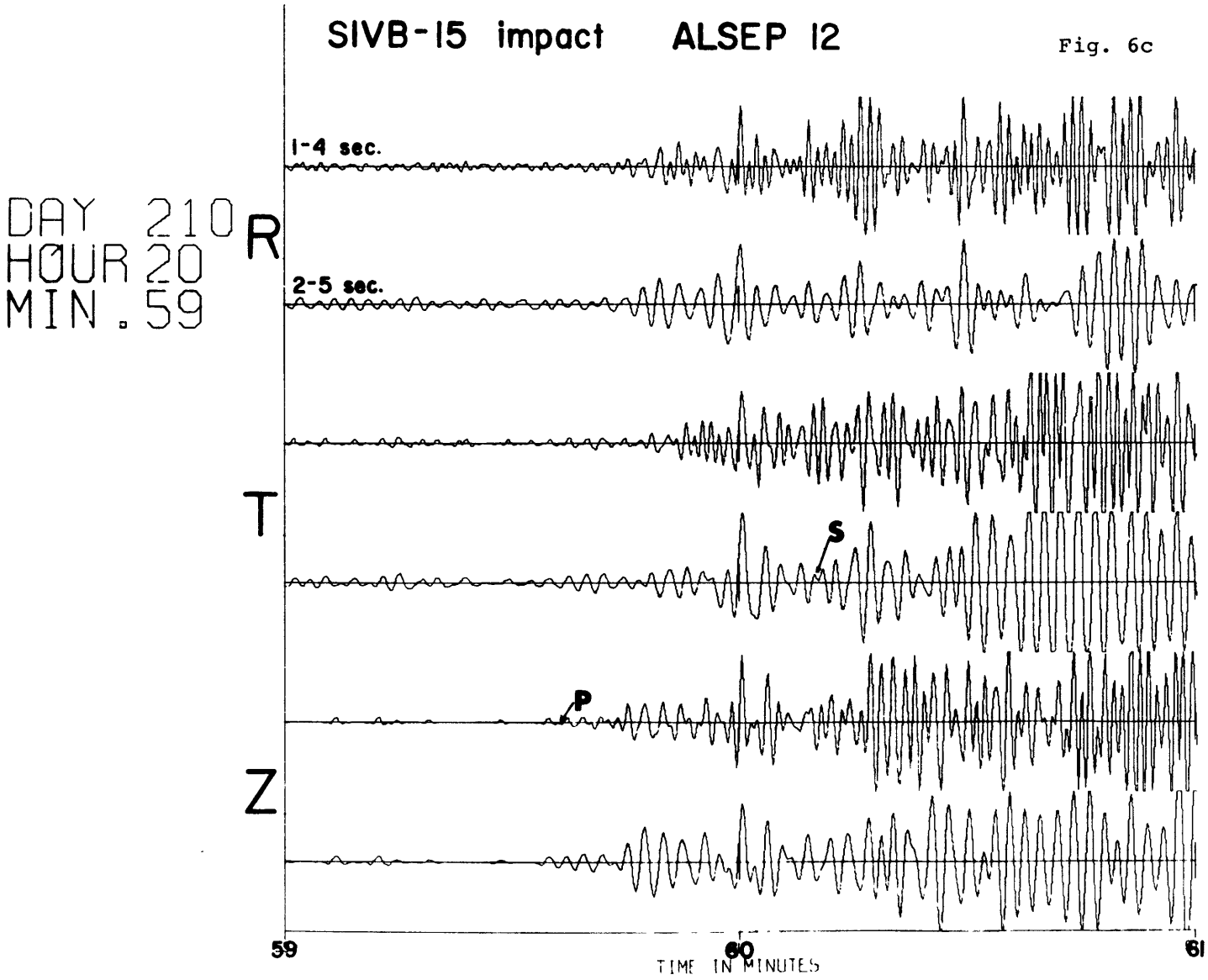
SIVB-15 impact ALSEP 12
Fig. 6c
DAY 210
HOUR 20
MIN. 59
1-4 sec.
2-5 sec.
R
T
Z
S
P
59
60
61
TIME IN MINUTES

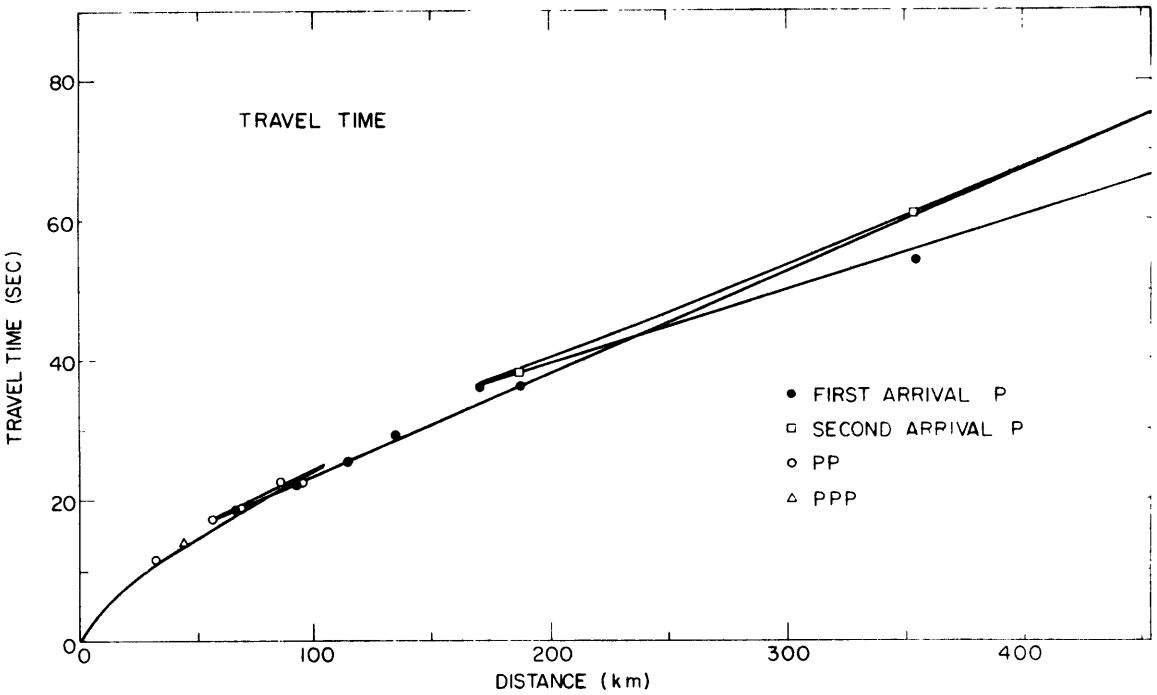
TRAVEL TIME
TRAVEL TIME (SEC)
DISTANCE (km)
FIRST ARRIVAL P
SECOND ARRIVAL P
PP
PPP

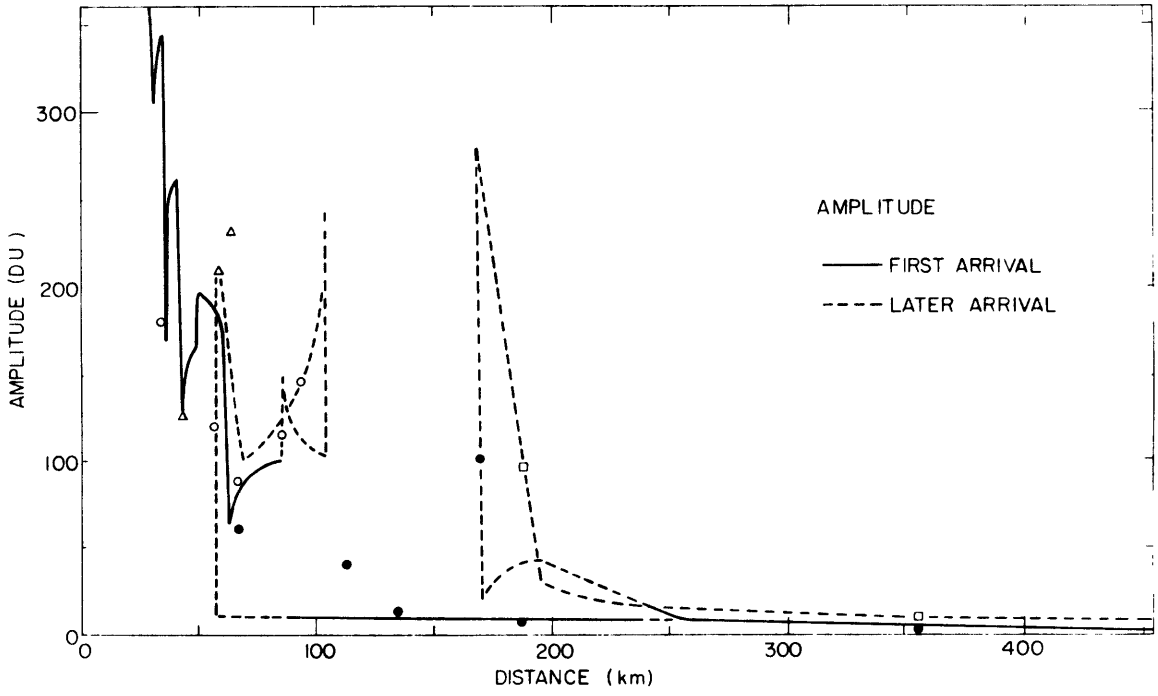
AMPLITUDE (DU)
DISTANCE (km)
AMPLITUDE
FIRST ARRIVAL
LATER ARRIVAL

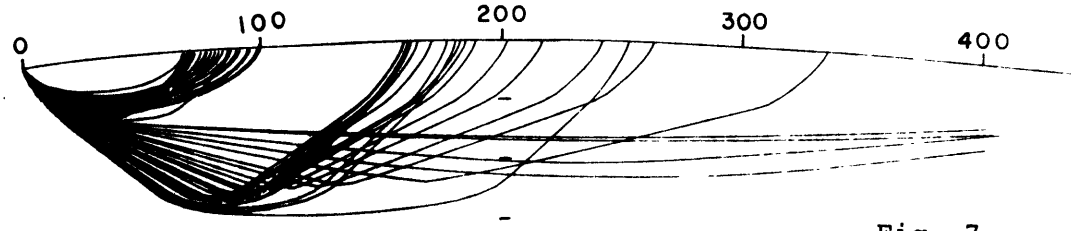
DEPTH 100 - km

Fig. 7

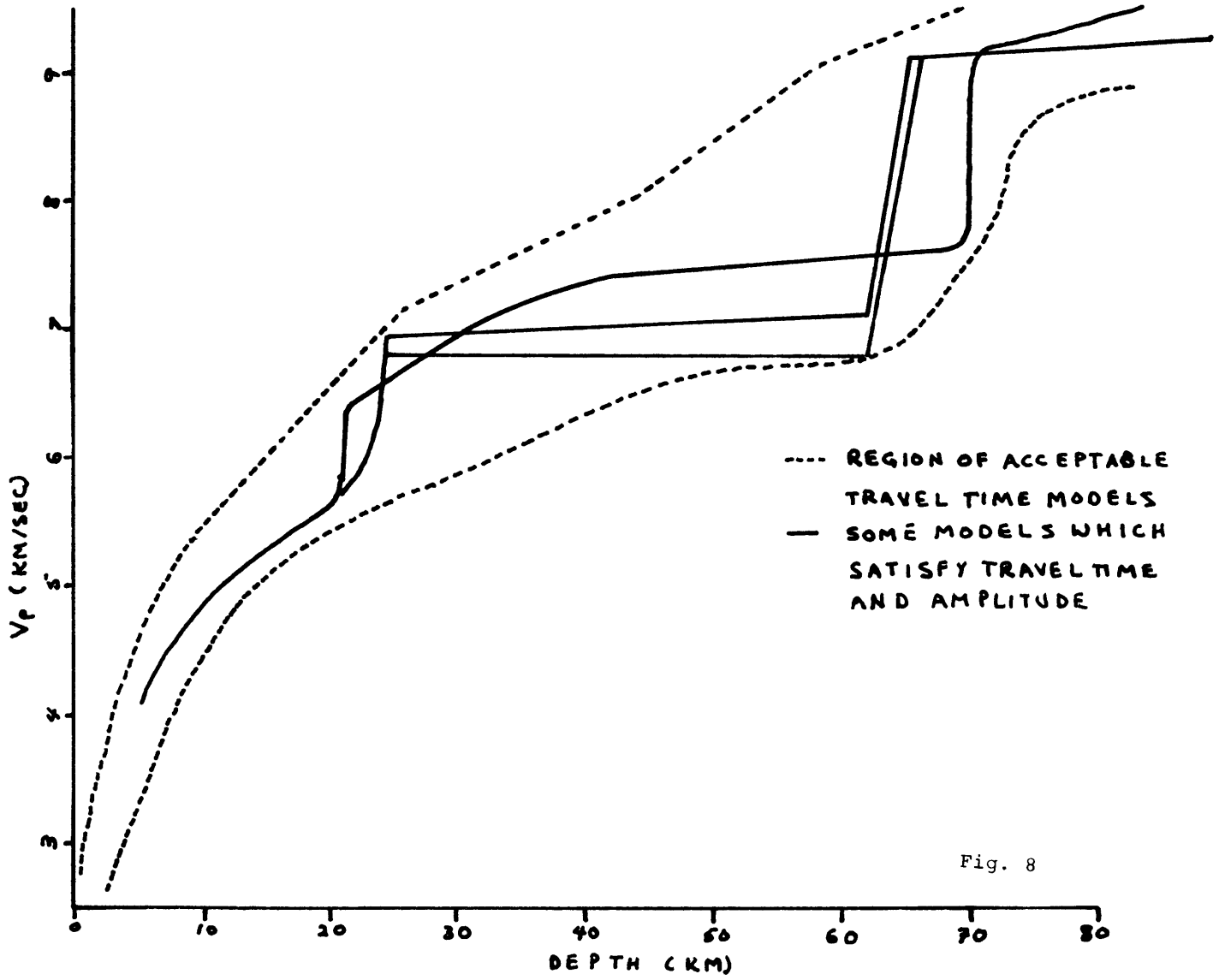
Vp (KM/SEC)
3
4
5
6
7
8
9
0
10
20
30
40
50
60
70
80
DEPTH (KM)
---- REGION OF ACCEPTABLE TRAVEL TIME MODELS
— SOME MODELS WHICH SATISFY TRAVEL TIME AND AMPLITUDE

Fig. 8

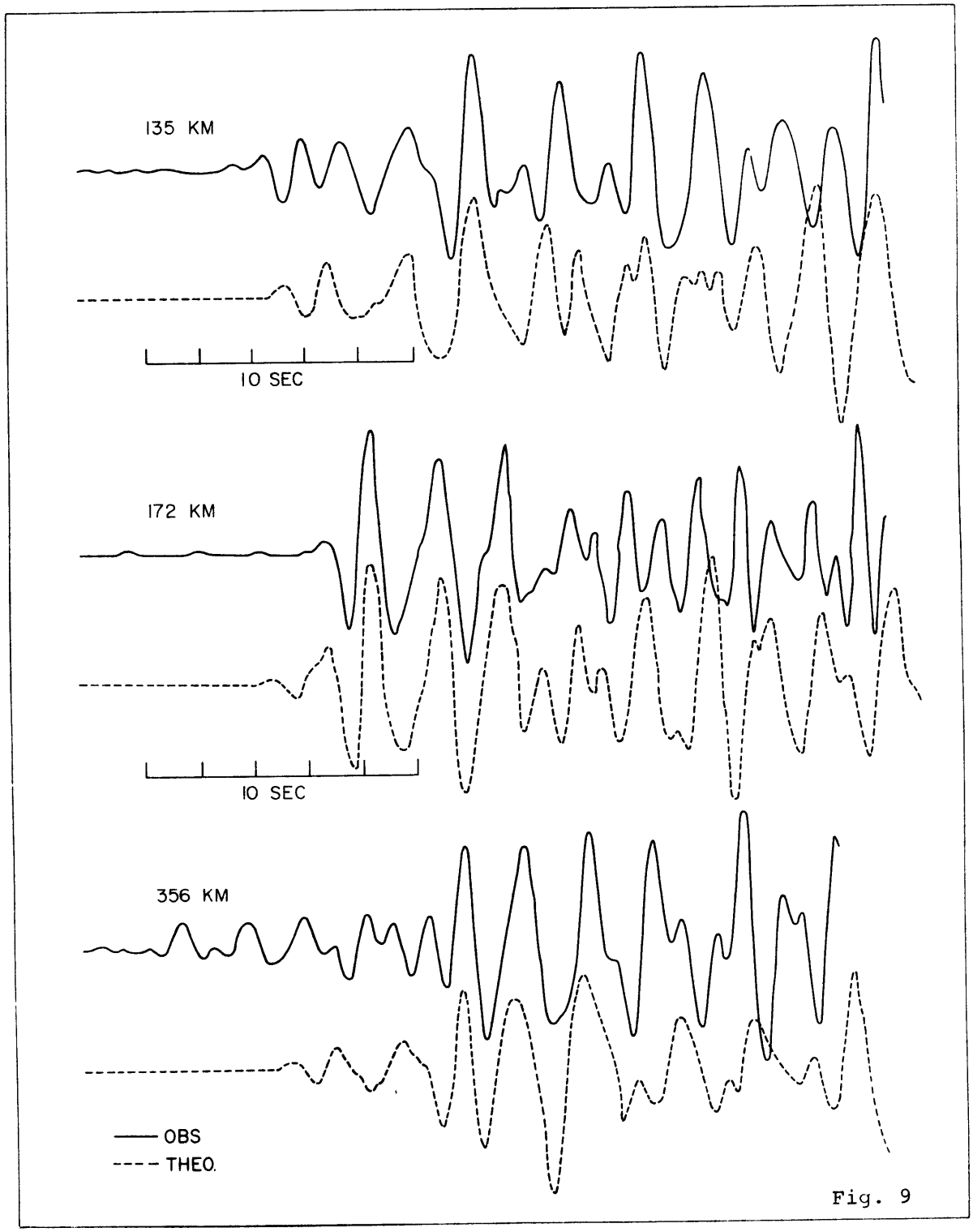

Fig. 9

Fig. 10

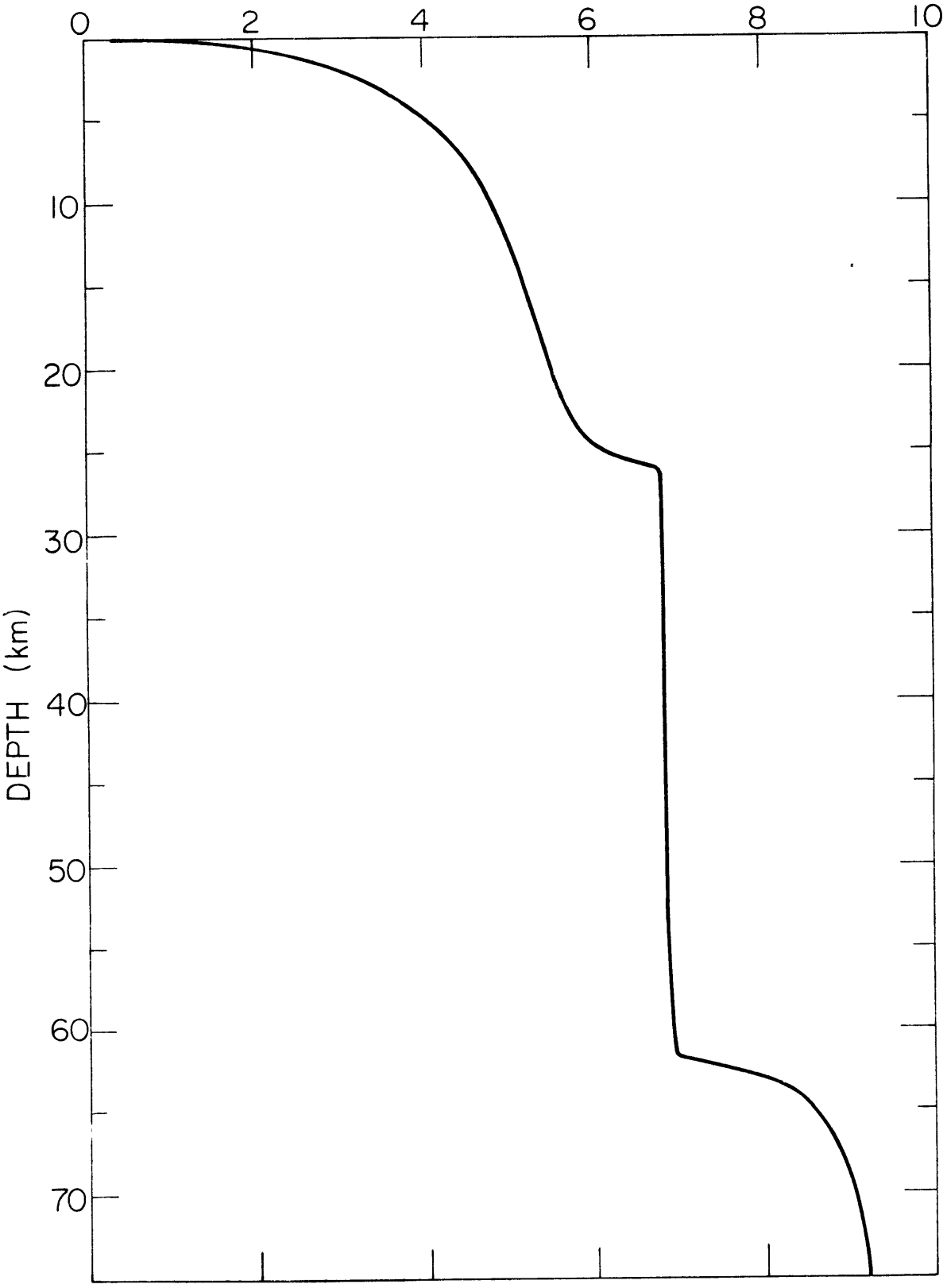

Fig. 11

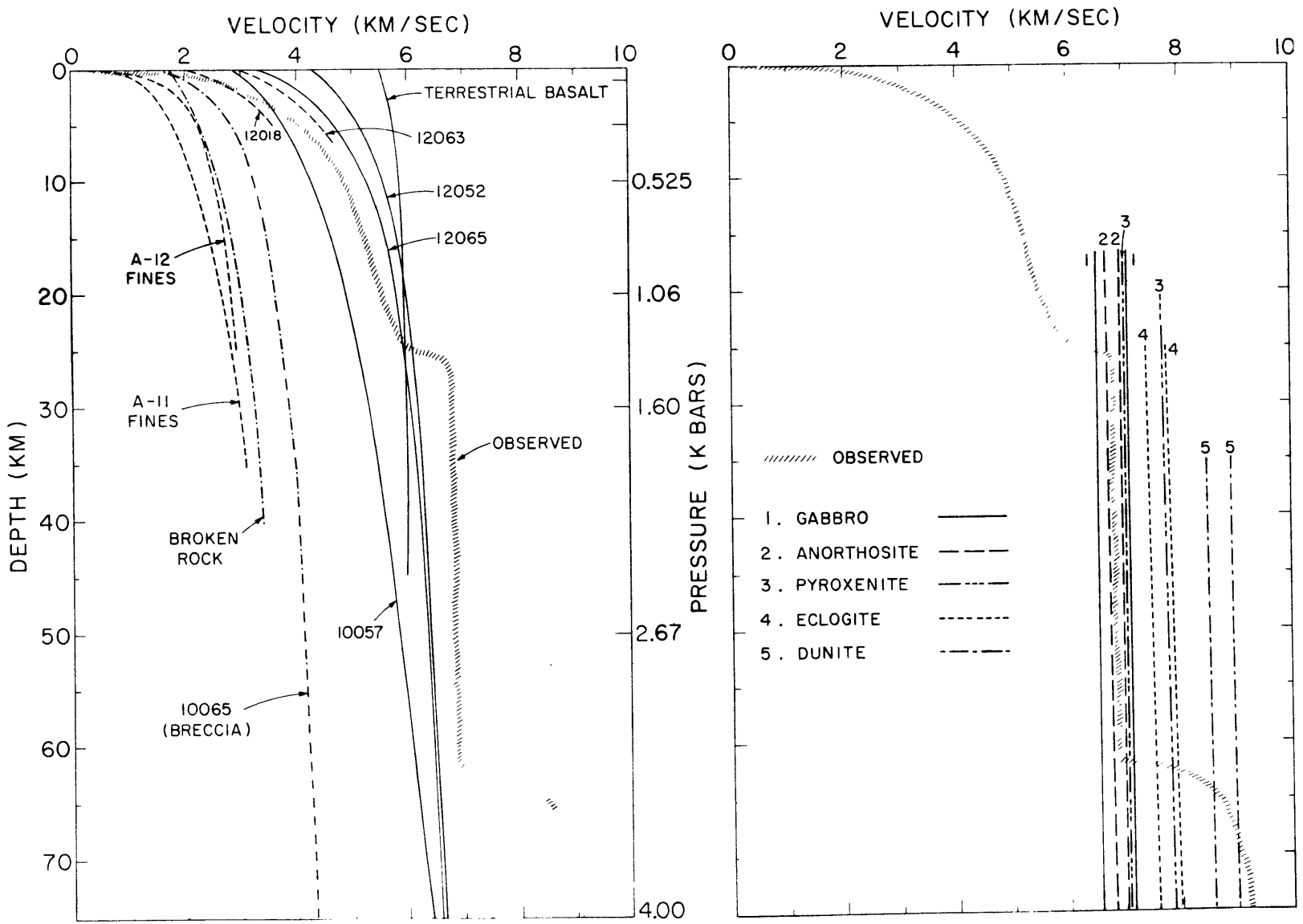
VELOCITY (KM/SEC)
0
2
4
6
8
10
DEPTH (KM)
0
10
20
30
40
50
60
70
PRESSURE (K BARS)
0.525
1.06
1.60
2.67
4.00
TERRESTRIAL BASALT
12018
12063
12052
12065
A-12 FINES
A-11 FINES
BROKEN ROCK
10057
10065 (BRECCIA)
OBSERVED
OBSERVED
1. GABBRO
2. ANORTHOSITE
3. PYROXENITE
4. ECLOGITE
5. DUNITE

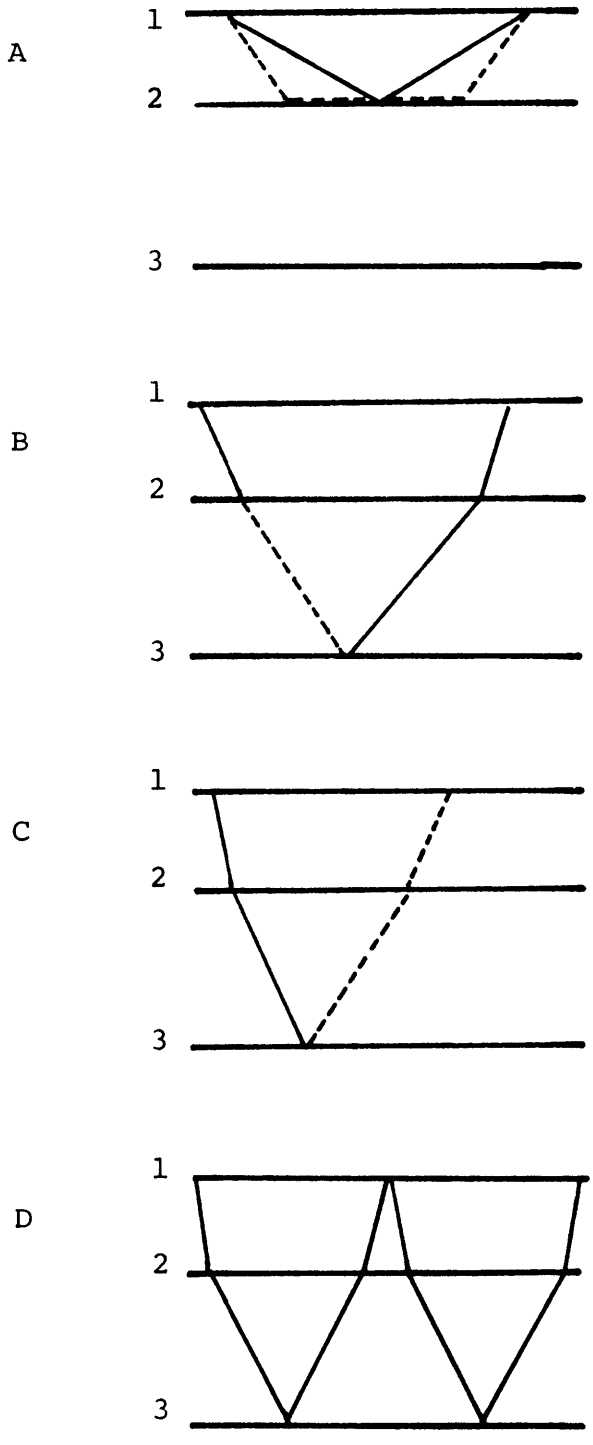
A
1
2
1^P2^P1
3
B
1
2
3
$1^P2^S3^P1$
C
1
2
3
1^P3^S1
D
1
2
3
$1^P3^P1^P3^P1$
P-WAVE
S-WAVE

Fig. 12

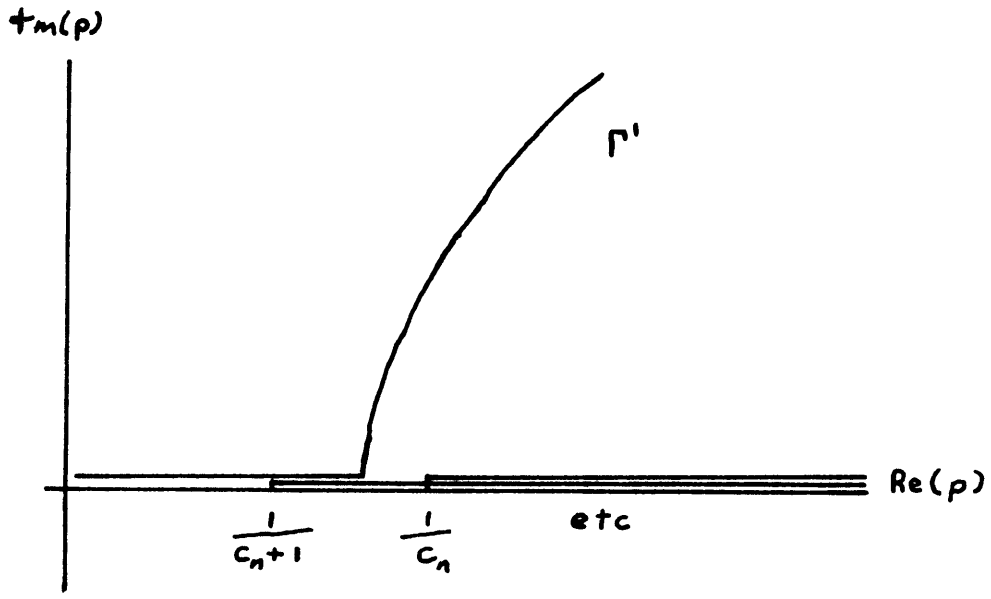

Fig. 13

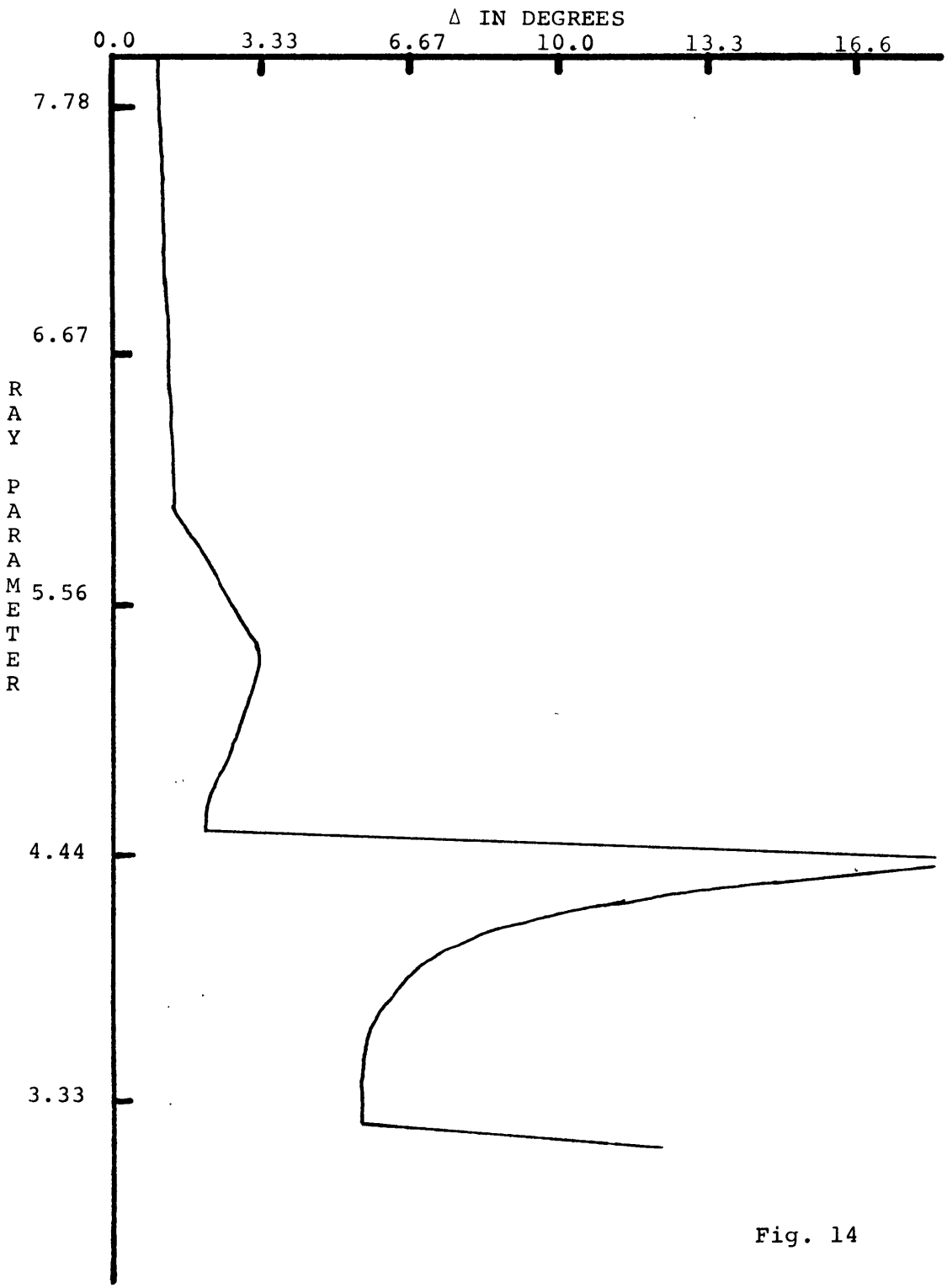
Δ IN DEGREES
0.0
3.33
6.67
10.0
13.3
16.6
7.78
6.67
5.56
4.44
3.33
RAY PARAMETER

Fig. 14